

1 Seawater pH reconstruction using boron isotopes in multiple planktonic foraminifera species with  
2 different depth habitats and their potential to constrain pH and pCO<sub>2</sub> gradients  
3  
4

5 Maxence Guillermic<sup>1,2</sup>, Sambuddha Misra<sup>3,4</sup>, Robert Eagle<sup>1,2</sup>, Alexandra Villa<sup>2,5</sup>, Fengming Chang<sup>6</sup>,  
6 Aradhna Tripathi<sup>1,2</sup>  
7  
8  
9  
10

11 <sup>1</sup> Department of Earth, Planetary, and Space Sciences, Department of Atmospheric and Oceanic  
12 Sciences, Institute of the Environment and Sustainability, UCLA, University of California – Los  
13 Angeles, Los Angeles, CA 90095 USA

14 <sup>2</sup> Laboratoire Géosciences Océan UMR6538, UBO, Institut Universitaire Européen de la Mer, Rue  
15 Dumont d'Urville, 29280, Plouzané, France

16 <sup>3</sup> Indian Institute of Science, Centre for Earth Sciences, Bengaluru, Karnataka 560012, India

17 <sup>4</sup> The Godwin Laboratory for Palaeoclimate Research, Department of Earth Sciences, University of  
18 Cambridge, UK

19 <sup>5</sup> Department of Geology, University of Wisconsin-Madison, Madison, WI 53706 USA

20 <sup>6</sup> Key Laboratory of Marine Geology and Environment, Institute of Oceanology, Chinese Academy of  
21 Sciences, Qingdao 266071, China  
22  
23  
24  
25  
26  
27  
28  
29  
30  
31  
32  
33  
34  
35  
36

37 Submitted to Biogeosciences  
38  
39  
40

41 \*Corresponding authors:

42 E-mail address: maxence.guillermic@gmail.com, atripati@ucla.edu  
43

44 **ABSTRACT**

45

46 Boron isotope systematics of planktonic foraminifera from core-top sediments and culture experiments have  
47 been studied to investigate the sensitivity of  $\delta^{11}\text{B}$  of calcite tests to seawater pH. However, our knowledge of the  
48 relationship between  $\delta^{11}\text{B}$  and pH remains incomplete for many taxa. Thus, to expand the potential scope of  
49 application of this proxy, we report  $\delta^{11}\text{B}$  data for 7 different species of planktonic foraminifera from sediment  
50 core-tops. We utilize a method for the measurement of small samples of foraminifera and calculate the  $\delta^{11}\text{B}$ -  
51 calcite sensitivity to pH for *Globigerinoides ruber*, *Trilobus sacculifer* (sacc or w/o sacc), *Orbulina universa*,  
52 *Pulleniatina obliquiloculata*, *Neogloboquadrina dutertrei*, *Globorotalia menardii* and *Globorotalia tumida*,  
53 including for unstudied core-tops and species. The sensitivity of  $\delta^{11}\text{B}_{\text{carbonate}}$  to  $\delta^{11}\text{B}_{\text{borate}}$  (eg.  
54  $\Delta\delta^{11}\text{B}_{\text{carbonate}}/\Delta\delta^{11}\text{B}_{\text{borate}}$ ) in core-tops is consistent with previous studies for *T. sacculifer* and *G. ruber* and close  
55 to unity for *N. dutertrei*, *O. universa* and combined deep-dwelling species. Deep-dwelling species closely follow  
56 the core-top calibration for *O. universa*, which is attributed to respiration-driven microenvironments, likely  
57 caused by light limitation and/or symbiont/host interactions. These taxa have diverse ecological preferences and  
58 are from sites that span a range of oceanographic regimes, including some that are in regions of air-sea  
59 equilibrium and others that are out of equilibrium with the atmosphere. Our data support the premise that  
60 utilizing boron isotope measurements of multiple species within a sediment core can be utilized to constrain  
61 vertical profiles of pH and  $\text{pCO}_2$  at sites spanning different oceanic regimes, thereby constraining changes in  
62 vertical pH gradients and yielding insights into the past behavior of the oceanic carbon pumps.

## 63 1. Introduction

64 The oceans are absorbing a substantial fraction of anthropogenic carbon emissions resulting in declining  
65 surface ocean pH (Fig. 1; IPCC, 2014). Yet there is a considerable uncertainty over the magnitude of future pH  
66 change in different parts of the ocean and the response of marine biogeochemical cycles to physio-chemical  
67 parameters (T, pH) caused by climate change (Bijma et al., 2002; Ries et al., 2009). Therefore, there is an  
68 increased interest in reconstructing past seawater pH (Hönisch and Hemming, 2004; Liu et al., 2009; Wei et al.,  
69 2009; Douville et al., 2010), in understanding spatial variability in aqueous pH and carbon dioxide ( $p\text{CO}_2$ )  
70 (Foster et al., 2008; Martinez-Boti et al., 2015b; Raitzsch et al., 2018), and in studying the response of the  
71 biological carbon pump utilizing geochemical proxies (Yu et al., 2007, 2010, 2016).

72 Although proxies for carbon cycle reconstruction are complex in nature (Pagani et al., 2005; Tripathi et  
73 al., 2009, 2011; Allen and Hönisch, 2012), the boron isotope composition of foraminiferal tests is emerging as  
74 one of the more robust tools (Hönisch et al., 2004, 2009; Ni et al., 2007; Foster et al., 2008, 2012; Bartoli et al.,  
75 2011; Henehan et al., 2013; Martinez-Boti et al., 2015b; Chalk et al., 2017). The study of laboratory-cultured  
76 foraminifera has demonstrated a systematic dependence of the boron isotope composition of tests on ambient pH  
77 (Sanyal et al., 1996, 2001; Henehan et al., 2013, 2016). Core-top measurements on globally distributed samples  
78 also show a  $\delta^{11}\text{B}$  sensitivity to pH with taxa-specific offsets from the theoretical fractionation line of borate ion  
79 (Rae et al., 2011; Henehan et al., 2016; Raitzsch et al., 2018).

80 Knowledge of seawater pH, in conjunction with constraints on one other carbonate system parameter  
81 (Total Alkalinity (TA), DIC (dissolved inorganic carbon),  $[\text{HCO}_3^-]$ ,  $[\text{CO}_3^{2-}]$ ), can be utilized to constrain aqueous  
82  $p\text{CO}_2$ . Application of empirical calibrations for boron isotopes, determined for select species of foraminifera  
83 from core-tops and laboratory cultures, has resulted in accurate reconstructions of  $p\text{CO}_2$  utilizing downcore  
84 samples from sites that are currently in quasi-equilibrium with the atmosphere at present.  $\delta^{11}\text{B}_{\text{carbonate}}$  based  
85 reconstructed values of  $p\text{CO}_2$  are analytically indistinguishable from ice core  $\text{CO}_2$  records (Hönisch et al., 2004,  
86 2009; Foster et al., 2008; Henehan et al., 2013; Chalk et al., 2017).

87 Therefore, the last decade has produced several studies aiming at reconstructing past seawater pH using  
88 boron isotopes to constrain atmospheric  $p\text{CO}_2$  in order understand the changes in the global carbon cycle  
89 (Hönisch et al., 2005, 2009; Foster et al., 2008, 2012, 2014; Seki et al., 2010; Bartoli et al., 2011; Henehan et al.,  
90 2013; Martinez-Boti et al., 2015a, 2015b; Chalk et al., 2017). In addition to reconstructing atmospheric  $p\text{CO}_2$ , in  
91 a few studies, the  $\delta^{11}\text{B}$  proxy has been applied to mixed-layer planktonic foraminifera at sites out of equilibrium  
92 with the atmosphere to constrain past air-sea fluxes (Foster et al., 2014; Martinez-Boti et al., 2015b). A small  
93 body of work has examined whether data for multiple species in core-top (Foster et al., 2008) and down-core  
94 samples could be used to constrain vertical profiles of pH through time (Palmer et al., 1998; Pearson and Palmer,  
95 1999; Anagnostou et al., 2016).

96 In this study, we make critical additions to the emerging pool of boron isotope data of core-top  
97 planktonic foraminifera from different oceanographic regimes, including data for species that have not  
98 previously been examined. We utilize a low-blank (15 pg B to 65 pg B), high precision (2sd on the international  
99 standard JCP-1 is 0.20 ‰, n=6)  $\delta^{11}\text{B}_{\text{carbonate}}$  analysis method (down to  $\sim 250 \mu\text{g CaCO}_3$ ), modified after Misra et  
100 al. (2014), to study multiple species of planktonic foraminifera from sediment core-tops that span a range of  
101 oceanographic regimes, including open-ocean oligotrophic settings and marginal seas. We constrain calibrations  
102 for different species, and compare results to published work (Foster et al., 2008; Henehan et al., 2013; Henehan

103 et al., 2016; Martinez-Boti et al., 2015b; Raitzsch et al., 2018). We also test whether these data support the  
104 application of boron isotope measurements of multiple species within a sediment core as a proxy for constraining  
105 vertical profiles of pH and pCO<sub>2</sub>.

106

## 107 **2. Background**

### 108 **2.1 Planktonic foraminifera as archives of seawater pH**

109 Planktonic foraminifera are used as archives of past environmental conditions within the mixed layer  
110 and thermocline, as their chemical composition is correlated with the physio-chemical parameters of their  
111 calcification environment (Ravelo and Fairbanks, 1992; Elderfield and Ganssen, 2000; Dekens et al., 2002;  
112 Anand et al., 2003; Sanyal et al., 2001; Ni et al., 2007; Henehan et al., 2013, 2015, 2016; Howes et al., 2017;  
113 Raitzsch et al., 2018). The utilization of geochemical data for multiple planktonic foraminifera species with  
114 different ecological preferences to constrain vertical gradients has been explored in several studies. The  
115 framework for such an approach was first developed using modern samples of planktonic foraminifera for  
116 oxygen isotopes, where it was proposed as a tool to constrain vertical temperature gradients and study physical  
117 oceanographic conditions during periods of calcification (Ravelo and Fairbanks, 1992).

118 Because planktonic foraminifera species complete their lifecycle in a particular depth habitat due to  
119 their ecological preference (Ravelo and Fairbanks, 1992; Farmer et al., 2007), it is theoretically possible to  
120 reconstruct water column profiles of pH using data from multiple taxa (Palmer and Pearson, 1998; Anagnostou  
121 et al., 2016). The potential use of an analogous approach to reconstruct past profiles of seawater pH was first  
122 highlighted by Palmer and Pearson (1998) on Eocene samples to constrain pH-depth gradients. However, in  
123 these boron isotope-based studies, it was assumed that boron isotope offset from seawater and foraminiferal  
124 carbonate were constant, which is an assumption not supported by subsequent studies (e.g., Hönisch et al., 2003;  
125 Foster et al., 2008; Henehan et al., 2013, 2016; Raitzsch et al., 2018; Rae, 2018). Furthermore, δ<sup>11</sup>B differences  
126 between foraminifera species inhabiting waters of the same pH makes the acquisition of more core-top and  
127 culture data essential for applications of the proxy.

128

### 129 **2.2 Boron systematics in seawater**

130 Boron is a conservative element in seawater with a long residence time (τ<sub>B</sub> ~ 14 Myr) (Lemarchand et  
131 al., 2002a). In seawater, boron exists as trigonal boric acid B(OH)<sub>3</sub> and tetrahedral borate ion B(OH)<sub>4</sub><sup>-</sup> (borate).  
132 The relative abundance of boric acid and borate ion is a function of the ambient seawater pH. At standard open  
133 ocean conditions (T = 25 °C and S = 35), the dissociation constant of boric acid is 8.60 (Dickson, 1990),  
134 implying that boron mainly exists in the form of boric acid in seawater. Since the pK<sub>B</sub> and seawater pH (e.g.,  
135 ~8.1, NBS) values are similar, it implies that small changes in seawater pH will induce strong variations in the  
136 abundance of the two boron species (Fig. 2).

137 Boron has two stable isotopes, <sup>10</sup>B and <sup>11</sup>B, with average relative abundances of 19.9 and 80.1 %,   
138 respectively. Variations in B isotope ratio are expressed in conventional delta (δ) notation:

139

$$140 \quad \delta^{11}\text{B} (\%) = 1000 \times \left( \frac{{}^{11}\text{B}/{}^{10}\text{B}_{\text{Sample}}}{{}^{11}\text{B}/{}^{10}\text{B}_{\text{NIST 951-a}}} - 1 \right) \quad (1)$$

141

142 where positive values represent enrichment in the heavy isotope  $^{11}\text{B}$ , and negative values enrichment in the light  
143 isotope  $^{10}\text{B}$ , relative to the standard reference material. Boron isotope values are reported versus the NIST SRM  
144 951 (Cantazaro et al., 1970).

145  $\text{B}(\text{OH})_3$  is enriched in  $^{11}\text{B}$  compared to  $\text{B}(\text{OH})_4^-$  with a constant offset between the two chemical  
146 species, within the range of physio-chemical variation observed in seawater, given by the fraction factor ( $\alpha$ ). The  
147 fractionation ( $\epsilon$ ) between  $\text{B}(\text{OH})_3$  and  $\text{B}(\text{OH})_4^-$  of  $27.2 \pm 0.6 \text{ ‰}$  has been empirically determined by Klochko et  
148 al., (2006) in seawater. Note, Nir et al. (2015) calculate this fractionation, using an independent method, to be  $26$   
149  $\pm 1 \text{ ‰}$ , which is within the analytical uncertainty of the Klochko et al. (2006) value. We use a fractionation  
150 factor of  $27.2 \text{ ‰}$  from Klochko et al. (2006) in this study.

151

### 152 **2.3 Boron isotopes in planktonic foraminifera calcite**

153 Many biogenic carbonate-based geochemical proxies are affected by “vital effects” or biological  
154 fractionations (Urey et al., 1951). The  $\delta^{11}\text{B}_{\text{carbonate}}$  in foraminifera exhibits species-specific offsets (see Rae et al.,  
155 2018 for review) compared to theoretical predictions for the boron isotopic composition of  $\text{B}(\text{OH})_4^-$  ( $\alpha=1.0272$ ,  
156 Klochko et al., 2006). As the analytical and technical aspects of boron isotope measurements have improved  
157 (Foster et al., 2008; Rae et al., 2011; Misra et al., 2014; Lloyd et al., 2018), evidence for taxonomic differences  
158 have not been eliminated, but have become increasingly apparent (Foster et al., 2008, 2018; Henehan et al 2013,  
159 2016; Foster et al., 2016; Rae et al., 2018; Raitzsch et al., 2018).

160 At present, culture and core-top calibrations have been published for several planktonic species  
161 including *Trilobatus sacculifer*, *Globigerinoides ruber*, *Globigerina bulloides*, *Neogloboquadrina pachyderma*,  
162 *Orbulina universa* (Foster et al., 2008; Henehan et al., 2013; Henehan et al., 2015; Sanyal et al., 1996; Sanyal et  
163 al., 2001). Although the boron isotopic composition of several species of foraminifera are now commonly used  
164 tools for reconstructing surface seawater pH, for other species, there is a lack of data constraining boron isotope  
165 sensitivity between foraminiferal carbonate and borate ion in seawater.

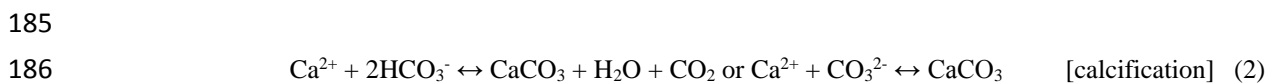
166

### 167 **2.4 Origin of biological fractionations in foraminifera**

168 Perforate foraminifera are calcifying organisms that maintain a large degree of biological control over  
169 their calcification space, and thus, mechanisms of biomineralization may be of significant importance in  
170 controlling the  $\delta^{11}\text{B}$  of the biogenic calcite. The biomineralization of foraminifera is based on seawater  
171 vacuolization (Erez, 2003; de Nooijer et al., 2014) with parcels of seawater being isolated by an organic matrix  
172 thereby creating a vacuole filled with seawater. Recent work has also demonstrated that even if the chemical  
173 composition of the reservoirs is modified by the organism, seawater is directly involved in the calcification  
174 process with vacuoles formed at the periphery of the shell (de Nooijer et al., 2014). Culture experiments by  
175 Rollion-Bard and Erez. (2010) have proposed that the pH at the site of biomineralization is elevated to an upper  
176 pH limit of  $\sim 9$  for the shallow-water, symbiont-bearing benthic foraminifera *Amphistegina lobifera*, which  
177 would support a pH modulation of a calcifying fluid in foraminifera. The extent to which these results apply to  
178 planktonic foraminiferal is not known, although pH modulation of calcifying fluid may influence the  $\delta^{11}\text{B}$  of  
179 planktonic foraminifera.

180 For taxa with symbionts, the microenvironment surrounding the foraminifera is chemically different  
181 from seawater due to photosynthetic activity (Jorgensen et al., 1985; Rink et al., 1998; Köhler-Rink and Kühl,

182 2000). Photosynthesis by the symbionts elevates the pH of the microenvironment (Jorgensen et al., 1985; Rink et  
183 al., 1998; Wolf-Gladrow et al., 1999; Köhler-Rink and Kühl, 2000), while calcification and respiration decrease  
184 it (Equation 2 and 3).



188  
189  $\delta^{11}\text{B}$  in foraminifera is primarily controlled by seawater pH, but is also dependent of the pH alteration of  
190 microenvironments due to calcification, respiration and symbiont photosynthesis.  $\delta^{11}\text{B}$  should therefore reflect  
191 the relative dominance of these processes and may account for species-specific  $\delta^{11}\text{B}$  offsets. Theoretical  
192 predictions from Zeebe et al. (2003) and foraminiferal data from Hönisch et al. (2003) explored the influence of  
193 microenvironment pH in  $\delta^{11}\text{B}$  signature of foraminifera. Their work also suggested that for a given species, there  
194 should be a constant offset observed between the boron isotope composition of foraminifera and borate ion over  
195 a large range of pH, imparting confidence in utilizing species-specific boron isotope data as a proxy for seawater  
196 pH.

197 Comparison of boron isotope data for multiple planktonic foraminiferal species indicate that taxa with  
198 high levels of symbiont activity such as *T. sacculifer* and *G. ruber* show higher  $\delta^{11}\text{B}$  values than the  $\delta^{11}\text{B}$  of  
199 ambient borate (Foster et al., 2008, Hennehan et al., 2013, Raitzsch et al., 2018). The sensitivities  
200 ( $\Delta\delta^{11}\text{B}_{\text{carbonate}}/\Delta\delta^{11}\text{B}_{\text{borate}}$ , hereafter referred to as the slope) of existing calibrations suggest a different species-  
201 specific sensitivity for these species compared to other taxa (Sanyal et al., 2001; Hennehan et al., 2013; Hennehan  
202 et al., 2015; Raitzsch et al., 2018). For example, *Orbulina universa* exhibits a lower  $\delta^{11}\text{B}$  than *in situ*  $\delta^{11}\text{B}$  values  
203 of borate ion (Hennehan et al., 2016), consistent with the species living deeper in the water column characterized  
204 by reduced photosynthetic activity.

205 It is possible that photosynthetic activity by symbionts might not be able to compensate for changes in  
206 calcification and/or respiration, leading to an acidification of the microenvironment. It is interesting to note that  
207 for *O. universa* the slope determined for the field-collected samples is not statistically different from unity ( $0.95$   
208  $\pm 0.17$ ) (Hennehan et al. 2016), while culture experiments report slopes of  $\leq 1$  for multiple species including *G.*  
209 *ruber* (Hennehan et al., 2013), *T. sacculifer* (Sanyal et al., 2001), and *O. universa* (Sanyal et al., 1999). More  
210 core-top and culture calibrations are needed to refine those slopes and understand if significant differences are  
211 observed, which is part of the motivation for this study.

## 212 213 **2.5 Planktic foraminifera depth and habitat preferences**

214 The preferred depth habitat of different species of planktonic foraminifera depends on their ecology,  
215 which in turn relies on the hydrographic conditions. For example, *G. ruber* is commonly found in the mixed  
216 layer (Fairbanks and Wiebe, 1980; Dekens et al., 2002; Farmer et al., 2007) during the summer (Deuser et al.,  
217 1981) whereas *T. sacculifer* is present in the mixed layer until mid-thermocline depths (Farmer et al., 2007)  
218 during spring and summer (Deuser et al., 1981, 1989). Specimens of *P. obliquiloculata* and *N. dutertrei* are  
219 abundant during winter months (Deuser et al., 1989), with an acme in the mixed layer (~60m) for *P.*  
220 *obliquiloculata*, and at mid-thermocline depths for *N. dutertrei* (Farmer et al., 2007). In contrast, *O. universa*  
221 tends to record annual average conditions within the mixed layer. Specimens of *G. menardii* calcify within the

222 seasonal thermocline (Fairbanks et al., 1982, Farmer et al., 2007, Regenberg et al., 2009), and in some regions in  
223 the upper thermocline (Farmer et al., 2007), and records annual temperatures. *G. tumida* is found at the lower  
224 thermocline or below the thermocline and records annual average conditions (Fairbanks and Wiebe, 1980;  
225 Farmer et al., 2007, Birch et al., 2013). Although the studies listed above showed evidence for species-specific  
226 living depth-habitat affinities, recent direct observations showed that environmental conditions (e.g. temperature,  
227 light) was locally responsible for the variability in the living depth of certain foraminifera species in the eastern  
228 North Atlantic (Rebotim et al., 2017). The same study showed evidence for a correspondence between living  
229 depth habitat and indirectly-derived calcification depth, supporting the approach utilized in this study.

230

### 231 **3. Materials and Methods**

232

#### 233 **3.1 Localities studied**

234 Core-top locations were selected to span a broad range of seawater pH, carbonate system parameters,  
235 and oceanic regimes. Samples from Atlantic Ocean (CD107-A), Indian Ocean (FC-01a and FC-02a), Arabian  
236 Sea (FC-13a and FC-12b) and Pacific Ocean (WP07-01, A14, and Ocean Drilling Program 806A and 807A)  
237 were analyzed; characteristics of the sites are summarized in Table 1 and S7, Fig. 3, and Fig. 4.

238 Atlantic site CD107-a (CD107 site A) was cored in 1997 by the Benthic Boundary Layer program  
239 (BENBO) (K.S. Black et al., 1997 - cruise report RRS Charles Darwin Cruise 107). Arabian Sea sites FC-12b  
240 (CD145 A150) and FC-13a (CD145 A3200) were retrieved by the *Charles Darwin* in the Pakistan Margin in  
241 2004 (B.J. Bett et al., 2003 - cruise report n°50 RRS Charles Darwin Cruise 145). A14 was recovered by box  
242 corer in the southern area of the South China Sea in 2012. Core WP07-01 was obtained from the Ontong Java  
243 Plateau using a giant piston corer during the Warm Pool Subject Cruise in 1993. Holes 806A and 807A were  
244 retrieved on Leg 130 by the Ocean Drilling Program (ODP). The top 10 cm of sediment from CD107-A have  
245 been radiocarbon dated to be Holocene <3 ky (Thomson et al., 2000). Samples from multiple box cores from  
246 Indian Ocean sites were radiocarbon dated as Holocene <7.3 ky (Wilson et al., 2012). Samples from western  
247 equatorial Pacific Site 806B, close to site WP07-01, are dated to between 7.3-8.6 ky (Lea et al., 2000). Arabian  
248 Sea and Pacific core-top samples were not radiocarbon dated but are assumed to be Holocene.

249

#### 250 **3.2 Species**

251 Around 50-100 foraminifera shells were picked from the 400-500 µm fraction size for *Globorotalia*  
252 *menardii* and *Globorotalia tumida*, >500 µm for *Orbulina universa*, from the 250-400 µm fraction size for  
253 *Trilobatus sacculifer* (w/o sacc, without sacc-like final chamber), *Trilobatus sacculifer* (sacc, sacc-like final  
254 chamber), *Globigerinoides ruber* (white, sensu stricto), *Neogloboquadrina dutertrei*, *Pulleniatina*  
255 *obliquiloculata*. The samples picked for analyses were visually well preserved.

256

#### 257 **3.3 Sample cleaning**

258 Briefly, picked foraminifera were gently cracked open, clay removed and checked for coarse-grained  
259 silicates. The next stages of sample processing and chemical separation were performed in a class 1000 clean lab  
260 equipped with boron-free HEPA filters. Samples were then cleaned using full reductive and oxidative cleaning  
261 (Boyle, 1981; Boyle and Keigwin, 1985; Barker et al., 2003). We utilized the reductive cleaning because some  
262 of the sites were not studied before, and previous comparisons of cleaning methods have shown there is no

263 impact on B/Ca (Misra et al., 2014b), nevertheless, it is possible that Fe-Mn oxide and hydroxides can result in  
264 non-negligible content of Mg and B contamination. Cleaned samples did not yield high Mn concentrations. We  
265 note that reductive cleaning leads to a decrease in Mg/Ca that in turn would result in a bias towards deeper CDs,  
266 which is not the case when we utilize non-Mg/Ca-based methodologies (i.e., CD<sub>1</sub> and CD<sub>3</sub>).

267 A final leaching step with 0.001N HCl was done before dissolution in 1N HCl. Hydrochloric acid was  
268 used to allow complete dissolution of the sample including Fe-Mn oxide and hydroxides if present. No matrix  
269 effect resulting from the mix HCl/HF was observed on the  $\delta^{11}\text{B}$ . Each sample was divided into two aliquots: an  
270 aliquot for boron purification and one aliquot for trace element analysis.

271

### 272 3.4 Reagents

273 Double-distilled HNO<sub>3</sub> and HCl acids (from Merck® grade) and a commercial bottle of HF Ultrapure  
274 grade were used at Brest. Double-distilled acids were used at Cambridge. All acids and further dilutions were  
275 prepared using double-distilled 18.2 M $\Omega$ .cm<sup>-1</sup> MQ water. Working standards for isotope ratio and trace element  
276 measurements were freshly diluted on a daily basis with the same acids used for sample preparation to avoid any  
277 matrix effects.

278

### 279 3.5 Boron isotopes

280 Boron purification for isotopic measurement was done utilizing microdistillation method developed by  
281 Gaillardet et al., (2001), for Ca-rich matrices by Wang et al., (2010) and adapted at Cambridge by Misra et al.,  
282 (2014a). 70  $\mu\text{L}$  of carbonate sample dissolved in 1N HCl was loaded on a cap of a clean fin legged 5 mL conical  
283 beaker upside down. The tightly closed beaker was put on a hotplate at 95°C for 15 hours. The beakers were  
284 taken off the hotplate and were allowed to cool for 15 min. The cap where the residue formed was replaced by a  
285 clean one. Then, 100  $\mu\text{L}$  of 0.5% HF were added to the distillate.

286 Boron isotopic measurements were carried out on a Thermo Scientific ®Neptune+ MC-ICP-MS at the  
287 University of Cambridge. Neptune+ was equipped with Jet interface and two 10<sup>13</sup>  $\Omega$  resistors. The instrumental  
288 setup included Savillex® 50 $\mu\text{l}/\text{min}$  C-flow self-aspirating nebulizer, single pass Teflon® Scott-type spray  
289 chamber constructed utilizing Savillex® column components, 2.0 mm Pt injector from ESI®, Thermo® Ni  
290 ‘normal’ type sample cone and ‘X’ type skimmer cones. Both isotopes of boron were determined utilizing 10<sup>13</sup>  $\Omega$   
291 resistors (Misra et al., 2014a; Lloyd et al., 2018).

292 The sample size for boron isotope analyses typically ranged from 10 ppb B (~5 ng B) to 20 ppb B  
293 samples (~10 ng B). Instrumental sensitivity for <sup>11</sup>B was 17 mV/ppb B (eg. 170 mV for 10ppb B) in wet plasma  
294 at 50 $\mu\text{l}/\text{min}$  sample aspiration rate. Intensity of <sup>11</sup>B for a sample at 10ppb B was typically 165mV  $\pm$  5mV closely  
295 matched the 170mV  $\pm$  5mV of the standard. Due to the low boron content of the samples extreme care was taken  
296 to avoid boron contamination during sample preparation and reduce memory effect during analysis. Procedural  
297 boron blanks ranged from 15pg B to 65 pg B (contributed to less than <1% of the sample signal). The acid blank  
298 during analyses was measured at  $\leq$  1mV on <sup>11</sup>B, meaning a contribution < 1% of the sample intensity, no  
299 memory effect was observed within and across sessions.

300 Analyses of external standards were done to ensure data quality. For  $\delta^{11}\text{B}$  measurements two carbonate  
301 standards were utilized: the JCp-1 (Geological Survey of Japan, Tsukuba, Japan) international standard (Gutjahr  
302 et al., 2014) and the NEP coral (Porites sp.,  $\delta^{11}\text{B} = 26.12 \pm 0.92$  ‰, 2SD, n=33 Holcomb et al., 2015 and Sutton



303 et al., 2018, Table S2) from University of Western Australia/Australian National University. A certified boric  
304 acid standard, the ERM<sup>®</sup> AE121 ( $\delta^{11}\text{B} = 19.9 \pm 0.6 \text{ ‰}$ , SD, certified) was used to monitor reproducibility and  
305 drift during each session (Vogl and Rosner, 2011; Foster et al., 2013; Misra et al., 2014). Results for the isotopic  
306 composition of the NEP standard are shown in Table S2, average values are  $\delta^{11}\text{B}_{\text{NEP}} = 25.70 \pm 0.93 \text{ ‰}$  (2SD,  
307  $n=22$ ) over different 7 analytical sessions with each number representing an ab-initio processed sample - this  
308 study). Our results are within error of published values of  $26.20 \pm 0.88 \text{ ‰}$  (2SD,  $n = 27$ ) and  $25.80 \pm 0.89 \text{ ‰}$   
309 (2SD,  $n = 6$ ) by Holcomb et al. (2015) and Sutton et al. (2018) respectively. Chemically cleaned J Cp-1 samples  
310 were measured at  $24.06 \pm 0.20$  (2SD,  $n=6$ ) and is within error of published values of  $24.37 \pm 0.32 \text{ ‰}$  and  $24.42 \pm$   
311  $0.28 \text{ ‰}$  by Holcomb et al. (2015) and Sutton et al. (2018) respectively.

312

### 313 3.6 Trace elements

314 The calcium concentration of each sample was measured on an ICP-AES<sup>®</sup> Ultima 2 HORIBA at the  
315 Pôle spectrometrie Océan (PSO), UMR6538 (Plouzané, France). Samples were then diluted to fixed calcium  
316 concentrations (typically 10 ppm or 30 ppm Ca) using 0.1 M HNO<sub>3</sub> & 0.3 M HF matching multi-element  
317 standards Ca concentration to avoid any matrix effects (Misra et al., 2014b), and levels in the remaining HCl  
318 (<1%) was negligible. Trace elements (e.g. X/Ca ratios) were analyzed on a Thermo Scientific<sup>®</sup> Element XR  
319 HR-ICP-MS at the PSO, Ifremer (Plouzané, France).

320 Trace element analyses were done at a Ca concentration of 10 or 30 ppm. The typical blanks for a 30  
321 ppm Ca session were:  $^7\text{Li} < 2\%$ ,  $^{11}\text{B} < 7\%$ ,  $^{25}\text{Mg} < 0.2\%$  and  $^{43}\text{Ca} < 0.02\%$ . Additionally, blanks for a 10 ppm Ca  
322 session were:  $^7\text{Li} < 2.5\%$ ,  $^{11}\text{B} < 10\%$ ,  $^{25}\text{Mg} < 0.4\%$  and  $^{43}\text{Ca} < 0.05\%$ . Due to strong memory effect for boron  
323 and instrumental drift on the Element XR, long sessions of conditioning were done prior analyses. Boron blanks  
324 were driven below 5% of signal intensity usually after 4 to 5 days of continuous analyses of carbonate samples.  
325 External reproducibility was determined on the consistency standard Cam-Wuellestorf (courtesy of the  
326 University of Cambridge) (Misra et al., 2014b), Table S3. Our X/Ca ratio measurements on the external standard  
327 Cam-Wuellestorf were all the time within error of the published value (Table S3) validating the robustness of  
328 our trace elements data. Analytical uncertainty of a single measurement was calculated from the reproducibility  
329 of the Cam-Wuellestorf, measured during a particular mass spectrometry session. The analytical uncertainties  
330 on the X/Ca ratios are: 0.4  $\mu\text{mol/mol}$  for Li/Ca, 7  $\mu\text{mol/mol}$  for B/Ca and 0.01  $\text{mmol/mol}$  for Mg/Ca (2SD,  
331  $n=31$ ) respectively.

332

### 333 3.7 Oxygen isotopes

334 Carbonate  $\delta^{13}\text{C}$  and  $\delta^{18}\text{O}$  were measured on a Gas Bench II coupled to a Delta V mass spectrometer at  
335 the stable isotope facility of Pôle spectrometrie Océan (PSO), Plouzané. Around 20 shells were weighed, crushed  
336 and clay removed. The recovered foraminifera were weighed in tubes and flushed with He gas. Samples were  
337 then digested in phosphoric acid and analyzed. Results were calibrated to the VPDB scale by international  
338 standard NBS19 and analytical precision on the in-house standard Ca21 was better than 0.11‰ for  $\delta^{18}\text{O}$  (1SD,  
339  $n=5$ ) and 0.03‰ for  $\delta^{13}\text{C}$  (1SD,  $n=5$ ).

340

### 341 3.8 Calcification depth determination

342 We utilized two different chemo-stratigraphic methods to estimate the calcification depth in this study  
343 (Table S6 and S7). The first method, commonly used in paleoceanography, utilizes  $\delta^{18}\text{O}$  measurements of the  
344 carbonate ( $\delta^{18}\text{O}_c$ ) to estimate calcification depths (referred to as  $\delta^{18}\text{O}$ -based calcification depths) (Schmidt et al.,  
345 2002; Mortyn et al., 2003; Sime et al., 2005; Farmer et al., 2007; Birsh et al., 2013). The second method utilizes  
346 Mg/Ca-based temperature estimates ( $T_{\text{Mg/Ca}}$ ) to constrain calcification depths (Quintana Krupinski et al., 2017).  
347 In both cases, the prerequisite was that vertical profiles of seawater temperature are available for different  
348 seasons in ocean atlases and cruise reports, and that hydrographic data and geochemical proxy signatures can be  
349 compared to assess the depth in the water column that represents the taxon's maximum abundance.

350 Because both methods have their uncertainties (in one case, use of taxon-specific calibrations, and in the  
351 other, analytical limitations), both estimates of calcification depth were compared to published values for the  
352 basin, and where available, for the same site (Table S6). To select which calcification depth to use for further  
353 calculations, we first looked at CD<sub>1</sub>, CD<sub>2</sub> and CD<sub>3</sub>. If, two CDs were similar we selected that one, if CD<sub>1</sub> and  
354 CD<sub>2</sub> were different we chose literature values (CD<sub>3</sub>) when available. For some less studied species, like *G.*  
355 *tumida*, *G. menardii* or *P. obliquiloculata*, CD<sub>3</sub> was not always available but showed good correspondence with  
356 our CD<sub>2</sub>, moreover due to availability of Mg/Ca-temperature taxon-specific calibrations we preferentially use  
357 CD<sub>2</sub> for those species.

358 We applied (based on uncertainties of our measurements) an uncertainty of  $\pm 10\text{m}$  for calcification  
359 depths  $> 70$  m and an uncertainty of  $\pm 20$  m when calcification depths  $< 70$  m. Direct observations of living  
360 depths of foraminifera remain limited. However, the depth uncertainties reported here are in line with the  
361 uncertainties calculated based on direct observations in the eastern North Atlantic which give a standard error on  
362 average living depths ranging from 6-22 m for the same species (Rebotim et al., 2017). The depth habitats  
363 utilized to derive *in situ* parameters are summarized in Table S7.

364

### 365 **3.9 $\delta^{11}\text{B}_{\text{borate}}$**

366 Two carbonate system parameters are needed to fully constrain the carbonate system. Following the  
367 approach of Foster et al., (2008) we used the GLODAP database (Key et al., 2004) corrected for anthropogenic  
368 inputs in order to estimate pre-industrial carbonate system parameters at each site. Temperature, salinity and  
369 pressure for each site are from the World ocean database 2013 (Boyer et al., 2013). We utilized the R<sup>®</sup> code in  
370 Henehan et al, (2016) (courtesy of Michael Henehan) to calculate the  $\delta^{11}\text{B}_{\text{borate}}$  and derive our calibrations.  
371 Uncertainty for  $\delta^{11}\text{B}_{\text{borate}}$  utilizing the code was similar to the one calculated by applying 2 standard deviations of  
372 the calculated  $\delta^{11}\text{B}_{\text{borate}}$  within the limits imposed by the calcification depth.

373 The Matlab<sup>®</sup> template provided by Zeebe and Wolf-Gladow, (2001) was used to calculate pCO<sub>2</sub> from  
374 TA; temperature, salinity and pressure were included into the calculations. Total boron was calculated from Lee  
375 et al., (2010), K<sub>1</sub> and K<sub>2</sub> were calculated from Mehrbach et al. (1973) refitted by Dickson and Millero (1987).

376 Statistical tests were made utilizing GraphPad<sup>®</sup> software, linear regressions for calibration where  
377 derived utilizing R<sup>®</sup> code in Henehan et al, (2016) (courtesy of Michael Henehan) with a k=500.

378

## 379 **4. Results**

380

### 381 **4.1 Depth habitat**

382 The calcification depths utilized in this paper are summarized in Tables S6 and S7, including a  
383 comparison of calcification depth determination methods. The calculated calcification depths are consistent with  
384 the ecology of each species and the hydrography of the sites. Specimens of *G. ruber* and *T. sacculifer* appear to  
385 be living in the shallow mixed layer (0-100 m), with *T. sacculifer* living or migrating deeper than *G. ruber*  
386 (down to 125 m). Specimens of *O. universa* and *P. obliquiloculata* are living in the upper thermocline; *G.*  
387 *menardii* is found in the upper thermocline until the thermocline depth specific to the location; *N. dutertrei* is  
388 living around the thermocline depth and specimens of *G. tumida* are found in the lower thermocline.

389 Data from both approaches implies that some species inhabit deeper environments in the Western  
390 Equatorial Pacific (WEP) relative to the Arabian Sea, which in turn are deeper-dwelling than in the Indian  
391 Ocean. In some cases, we find evidence for differences in habitat depth of up to ~100m between the WEP and  
392 the Arabian Sea. This trend is observed for *G. ruber* and *T. sacculifer*, but not for *O. universa*.

393 Some differences in calcification depth are observed between the two calcification depth determination  
394 methods. These differences might be due to the choice of calibrations. Alternatively, our uncertainties for  $\delta^{18}\text{O}$   
395 implies larger uncertainties on the calcification depth determination using this approach, compared to Mg/Ca  
396 measurements.

397

## 398 4.2 Empirical calibrations of foraminiferal $\delta^{11}\text{B}_{\text{carbonate}}$ to $\delta^{11}\text{B}_{\text{borate}}$

399 Results for the different species analyzed in this study are presented in Fig. 5, Fig. 6 and summarized in  
400 Table 2; additionally, published calibrations for comparison are summarized in Table 3.

401

### 402 4.2.1 *G. ruber*

403 Samples were picked from the 250-300  $\mu\text{m}$  fraction, except for the WEP sites where foraminifera shells  
404 were picked from the 250-400  $\mu\text{m}$  fraction. Weight per shell averaged  $11 \pm 4 \mu\text{g}$  (n=4, SD) although the weight  
405 was not measured on the same sub-sample analyzed for  $\delta^{11}\text{B}$  and trace elements or at the WEP sites. In  
406 comparison to literature, the size fraction used for this study was smaller: Foster et al. (2008) used the 300-  
407 355 $\mu\text{m}$  fraction, Henahan et al. (2013) utilized multiple size fractions (250-300, 250-355, 300-355, 355-400 and  
408 400-455  $\mu\text{m}$ ) and Raitzsch et al. (2018) used the 315-355  $\mu\text{m}$  fraction.

409 Our results for *G. ruber* (Fig. 5) are in close agreement with published data from other core-tops,  
410 sediment traps, tows, and culture experiments for  $\delta^{11}\text{B}_{\text{borate}} > 19 \text{‰}$  (Foster et al., 2008, Henahan et al., 2013,  
411 Raitzsch et al., 2018). However, the two datapoints from  $\delta^{11}\text{B}_{\text{borate}} < 19 \text{‰}$  are lower compared to previous studies.  
412 Elevated  $\delta^{11}\text{B}_{\text{carbonate}}$  values relative to  $\delta^{11}\text{B}_{\text{borate}}$  has been explained by the high photosynthetic activity (Hönisch  
413 et al., 2003; Zeebe et al., 2003). Three calibrations have been derived (Table 3). Linear regression on our data  
414 alone yields a slope of 1.12 ( $\pm 1.67$ ). While this regression is not significantly different from a 1:1 line, the  
415 uncertainty term are significant given limited data in our study. Therefore, the sensitivity of  $\delta^{11}\text{B}_{\text{carbonate}}$  to  
416  $\delta^{11}\text{B}_{\text{borate}}$  of our linear regression is not statistically different from 1, the uncertainty on this regression is  
417 important due to our small dataset, thus not inconsistent with the low sensitivity trend of the culture experiments  
418 from Sanyal et al., (2001) or Henahan et al., (2013). The second calibration made compiling all data from  
419 literature shows a sensitivity similar (e.g. 0.46 ( $\pm 0.34$ )) to the one recently published by Raitzsch et al., (2018)  
420 (e.g. 0.45 ( $\pm 0.16$ ), Table 3). The third linear regression made only on data from the 250-400  $\mu\text{m}$  fraction from  
421 our study and from the 250-300  $\mu\text{m}$  from Henahan et al. (2013) yields a slope of 0.58 ( $\pm 0.91$ ) similar to culture

422 experiments from Henehan et al., (2013) (e.g.  $0.6 (\pm 0.16)$ , Table 3). This third calibration is offset by  $\sim -0.4 \text{ ‰}$   
423 ( $p > 0.05$ ) compared to culture calibration from Henehan et al. (2013). The variability in our weight per shell  
424 based data from Henehan et al., (2013) can potentially imply a deviation down to  $1 \text{ ‰}$  relative to its calibration  
425 line, which can be in line with the maximum deviation observed in our data ( $\sim 1.2 \text{ ‰}$ ) and not inconsistent with a  
426 size effect explaining the offset in our calibration.

427

#### 428 **4.2.2 *T. sacculifer***

429  $\delta^{11}\text{B}_{\text{carbonate}}$  results for *T. sacculifer* (sacc and w/o sacc) (Fig. 5) are compared to published data (Foster  
430 et al., 2008; Martinez-Boti et al., 2015b, Raitzsch et al., 2018). Results for *T. sacculifer* are in good agreement  
431 with the literature and exhibit higher  $\delta^{11}\text{B}_{\text{carbonate}}$  compared to expected  $\delta^{11}\text{B}_{\text{borate}}$  at their collection location. A  
432 linear regression through our data alone yields a slope of  $1.3 \pm 0.2$  but is not statistically different to the results  
433 from Martinez-Boti et al., (2015b) (Table 3), ( $p > 0.05$ ). However, when compiled with published data using the  
434 bootstrap method a slope of  $0.83 \pm 0.48$  is calculated, with a large uncertainty given the variability in the data. It  
435 is also noticeable that *T. sacculifer* (w/o sacc) samples from the WEP have a  $\delta^{11}\text{B}_{\text{carbonate}}$  close to expected  
436  $\delta^{11}\text{B}_{\text{borate}}$  and are significantly lower compared to the combined *T. sacculifer* of other sites ( $p = 0.01$ , unpaired t-  
437 test). When doing the regression using data from the 250-400  $\mu\text{m}$  fraction, our results are not significantly  
438 different from the regression through data that combine all size fractions (Fig. 5).

439

#### 440 **4.2.3 *O. universa* and deeper-dwelling species: *N. dutertrei*, *P. obliquiloculata*, *G. menardii* and *G. tumida***

441 Our results for *O. universa* (Fig. 5), *N. dutertrei*, *P. obliquiloculata*, *G. menardii* and *G. tumida* (Fig. 6)  
442 exhibit lower  $\delta^{11}\text{B}_{\text{carbonate}}$  compared to the expected  $\delta^{11}\text{B}_{\text{borate}}$  at their collection location. These data for *O.*  
443 *universa* are not statistically different from the Henehan et al. (2016) calibration ( $p > 0.05$ ). Our results for *N.*  
444 *dutertrei* expand upon the initial measurements presented in Foster et al., (2008). The different environments  
445 experienced by *N. dutertrei* in our study permit us to extend the range and derive a calibration for this species;  
446 the slope is close to unity ( $0.93 \pm 0.55$ ), and is not significantly different ( $p > 0.05$ ) from the *O. universa*  
447 calibration previously reported by Henehan et al. (2016) (e.g.  $0.95 \pm 0.17$ ). The data for *P. obliquiloculata*  
448 exhibits the largest offset from the theoretical line. The range of  $\delta^{11}\text{B}_{\text{borate}}$  from the samples we have of *G.*  
449 *menardii* and *G. tumida* is not sufficient to derive calibrations, but the points are in good agreement with the *N.*  
450 *dutertrei* calibration and Henehan et al. (2016) calibration for *O. universa*.

451 For *O. universa* and all deep-dwelling species, the slopes are not statistically different from Henehan et  
452 al. (2016) ( $p > 0.05$ ) and are close to unity. If data for deep-dwelling foraminiferal species are pooled together  
453 with each other and with data from Henehan et al., (2016) and Raitzsch et al., (2018), we calculate a slope of  $0.95$   
454 ( $\pm 0.13$ ) ( $R^2 = 0.7987$ ,  $p < 0.0001$ ); if only our data are used, we calculate a slope that is not significantly different  
455 ( $0.82 \pm 0.27$ ;  $p < 0.05$ ). However, it remains premature to assume that a unique calibration with a slope of  $\sim 0.9$   
456 can be used for all deeper-dwelling species; more data is needed for *P. obliquiloculata*, *G. menardii* and *G.*  
457 *tumida* to robustly test this assertion.

458

#### 459 **4.2.4 Comparison of core-top and culture data**

460 The data for *G. ruber* and *T. sacculifer* from the core-tops we measured are broadly consistent with  
461 previous published results. The calibrations between these core-top derived estimates and culture experiments

462 are not statistically different due to small datasets and uncertainties on the linear regressions (Henehan et al.,  
463 2013; Marinez-Boti et al., 2015; Raitzsch et al., 2018; Table 3). The sensitivities of the species analyzed are not  
464 statistically different and are close to unity.

465

### 466 4.3 B/Ca ratios

467 B/Ca ratios are presented in Table 2 and Fig. 7. B/Ca data are species-specific and consistent with  
468 previous work (e.g., compiled in Henehan et al., 2016) with ratios higher for *G. ruber* > *T. sacculifer* (sacc) > *T.*  
469 *sacculifer* (w/o sacc) > *P. obliquiloculata* > *O. universa* >> *G. menardii* > *N. dutertrei* > *G. tumida* > *G. inflata*  
470 > *N. pachyderma* > *G. bulloides* (Fig. 7). This study supports species-specific B/Ca ratios as previously  
471 published (Yu et al., 2007; Tripathi et al., 2009, 2011; Allen and Hönisch, 2012; Henehan et al., 2016).  
472 Differences between surface- and deep-dwelling foraminifera are observed, with lower values and a smaller  
473 range for the deeper-dwelling taxa (58-126  $\mu\text{mol/mol}$  vs 83-190  $\mu\text{mol/mol}$  for shallow dwellers), however, the  
474 trend for the surface-dwellers can also be driven by interspecies B/Ca variability. The B/Ca data for deep-  
475 dwelling taxa exhibits a significant correlation with  $[\text{B}(\text{OH})_4^-]/[\text{HCO}_3^-]$  ( $p < 0.05$ ), but no correlation with  
476  $\delta^{11}\text{B}_{\text{carbonate}}$  and temperature (Fig. S3). Surface-dwelling species have B/Ca ratios that exhibit significant  
477 correlations with  $[\text{B}(\text{OH})_4^-]/[\text{HCO}_3^-]$ ,  $\delta^{11}\text{B}_{\text{carbonate}}$  and temperature. The sensitivity of B/Ca to  $[\text{B}(\text{OH})_4^-]/[\text{HCO}_3^-]$   
478 is lower for deep-dwelling species compared to surface dwelling species. When all the B/Ca data are compiled,  
479 significant trends are observed with  $[\text{B}(\text{OH})_4^-]/[\text{HCO}_3^-]$ ,  $\delta^{11}\text{B}_{\text{carbonate}}$  and temperature (Fig. S3). When comparing  
480 data from all sites together, a weak decrease in B/Ca with increasing calcification depth is observed ( $R^2=0.11$ ,  
481  $p < 0.05$ , Fig. S4). A correlation also exists between B/Ca and the water depths of the cores (not significant, Fig.  
482 S4).

483

## 484 5. Discussion

485

### 486 5.1 Sources of uncertainty relating to depth habitat and seasonality at studied sites

487

#### 488 5.1.1 Depth habitats and $\delta^{11}\text{B}_{\text{borate}}$

489 Because foraminifera will record ambient environmental conditions during calcification, the accurate  
490 characterization of *in situ* data is needed not only for calibrations, but also to understand the reconstructed record  
491 of pH or  $p\text{CO}_2$ . The species we examined are ordered here from shallower to deeper depth habitats: *G. ruber* > *T.*  
492 *sacculifer* (sacc) > *T. sacculifer* (w/o sacc) > *O. universa* > *P. obliquiloculata* > *G. menardii* > *N. dutertrei* > *G.*  
493 *tumida* (this study; Birch et al., 2013; Farmer et al., 2007), although the specific water depth will vary depending  
494 on the hydrology of the site (Kemle-von Mücke and Oberhänsli, 1999). We note that calculation of absolute  
495 calcification depths can be challenging in some cases as many species often transition to deeper waters at the end  
496 of their life cycle prior to gametogenesis (Steinhardt et al., 2015).

497 We find that assumptions about the specific depth habitat a species of foraminifera is calcifying over, in  
498 a given region, can lead to differences of a few per mil in calculated isotopic compositions of borate (Fig. 4).  
499 Hence this can cause a bias in calibrations if calcification depths are assumed instead of being calculated (i.e.,  
500 with  $\delta^{18}\text{O}$  and/or Mg/Ca). Factors including variations in thermocline depth can impact depth habitats for some  
501 taxa. At the sites we examined, most of the sampled species live in deeper depth habitats in the WEP relative to

502 the Indian Ocean, which in turn is characterized by deeper depth habitats than in the Arabian Sea. In the tropical  
503 Pacific, *T. sacculifer* is usually found deeper than *G. ruber* except at sites characterized by a shallow  
504 thermocline, in which case both species tend to overlap their habitat (e.g., ODP Site 806 in the WEP which has a  
505 deeper thermocline than at ODP Site 847 in the Eastern Equatorial Pacific; EEP) (Rickaby et al., 2005). The  
506 difference in depth habitats for *T. sacculifer* and *N. dutertrei* between the WEP and EEP can be as much as  
507 almost 100 m (Rickaby et al., 2005).

508

### 509 **5.1.2 Seasonality and *in situ* $\delta^{11}\text{B}_{\text{borate}}$**

510 As discussed by Raitzsch et al., (2018), depending of the study area, foraminiferal fluxes can change  
511 throughout the year, so seasonality can have a major impact on hydrographic carbonate parameters calculations  
512 for any given water depth. We therefore recalculated the theoretical  $\delta^{11}\text{B}_{\text{borate}}$  using seasonal data for temperature  
513 and salinity and annual values for TA and DIC for each depth at each site. The GLODAP (2013) database does  
514 not provide seasonal TA or DIC values.

515 The low sensitivity of  $\delta^{11}\text{B}_{\text{borate}}$  to temperature and salinity means that calculated  $\delta^{11}\text{B}_{\text{borate}}$  for each  
516 water depth at our sites were not strongly impacted (Fig. S1). Thus, these findings support Raitzsch et al. (2018),  
517 who concluded that calculated  $\delta^{11}\text{B}_{\text{borate}}$  values corrected for seasonality was within error of non-corrected values  
518 for each water depth. As Raitzsch et al, (2018) highlight, seasonality might be more important at high latitude  
519 sites where seasonality is more marked, however, the seasonality of primary production will also be more tightly  
520 constrained due to the seasonal progression of winter light limitation and intense vertical mixing and summer  
521 nutrient limitation.

522 Data for our sites suggests that most  $\delta^{11}\text{B}_{\text{borate}}$  variability we observe does not come from seasonality but  
523 from the assumed water depths for calcification. With the exception of a few specific areas such as the Red Sea  
524 (Henehan et al., 2016, Raitzsch et al., 2018), at most sites examined, seasonal  $\delta^{11}\text{B}_{\text{borate}}$  at a fixed depth does not  
525 vary by more than  $\sim 0.2\%$ . We conclude that seasonality has a relatively minor impact on the carbonate system  
526 parameters at the sites we examined.

527

### 528 **5.2 $\delta^{11}\text{B}$ , microenvironment pH and depth habitats**

529 It is common for planktonic foraminifera to have symbiotic relationships with algae (Gast and Caron,  
530 2001; Shaked and de Vargas, 2006). The family Globigerinidae, including *G. ruber*, *T. sacculifer* and *O.*  
531 *universa*, commonly have dinoflagellate algal symbionts (Anderson and Be, 1976; Spero, 1987). The families  
532 Pulleniatinidae and Globorotaliidae (e.g. *P. obliquiloculata*, *G. menardii* and *G. tumida*) have chrysophyte algal  
533 symbionts (Gastrich, 1988) and *N. dutertrei* hosts pelagophyte symbionts (Bird et al., 2018). The relationship  
534 between the symbionts and the host is complex. Nevertheless, this symbiotic relationship provides energy  
535 (Hallock, 1981b) and promotes calcification in foraminifera (Duguay, 1983; Erez et al., 1983) by providing  
536 inorganic carbon to the host (Jorgensen et al., 1985).

537 There are several studies indicating that the  $\delta^{11}\text{B}$  signatures in foraminiferal calcite reflect  
538 microenvironment pH (Jorgensen et al., 1985; Rink et al., 1998; Köhler-Rink and Köhl, 2000, Hönisch et al.,  
539 2003; Zeebe et al., 2003). Foraminifera with high photosynthetic activity and symbiont density, such as *G. ruber*  
540 and *T. sacculifer*, are expected to have a microenvironment pH higher than ambient seawater, and a  $\delta^{11}\text{B}_{\text{carbonate}}$   
541 higher than expected  $\delta^{11}\text{B}_{\text{borate}}$ , which is the case in our study (Foster et al., 2008, Henehan et al., 2013, Raitzsch

542 et al., 2018). We also observed in our study that *N. dutertrei*, *G. menardii*, *P. obliquiloculata* and *G. tumida*  
543 record a lower pH than ambient seawater, with  $\delta^{11}\text{B}_{\text{carbonate}}$  lower than expected  $\delta^{11}\text{B}_{\text{borate}}$ , and suggest the results  
544 are consistent with lower photosynthetic activity compared to the aforementioned mixed-dweller species. These  
545 observations, based on  $\delta^{11}\text{B}_{\text{carbonate}}$  measurements, are in line with direct observations from Tagaki et al. (2019)  
546 that show dinoflagellate-bearing foraminifera (*G. ruber*, *T. sacculifer* and *O. universa*) tend to have a higher  
547 symbiont density and photosynthesis activity while *P. obliquiloculata*, *G. menardii* and *N. dutertrei* have lower  
548 symbiont density and *P. obliquiloculata*, *N. dutertrei* have the lowest photosynthetic activity. In the same study,  
549 *P. obliquiloculata* exhibited minimum symbiont densities and levels of photosynthetic activity which may  
550 explain why it exhibited the lowest microenvironment pH, as recorded by  $\delta^{11}\text{B}$ .

551 Based on the observations of Tagaki et al. (2019), we can assume that the low  $\delta^{11}\text{B}$  of *O. universa* and  
552 *T. sacculifer* (w/o sacc) from the WEP is explained by low photosynthetic activity. It has been shown for *T.*  
553 *sacculifer* and *O. universa* that symbiont photosynthesis increases with higher insolation (Jorgensen et al., 1985;  
554 Rink et al., 1998) and the photosynthetic activity is therefore a function of the light level the symbionts received.  
555 This is, in a natural system, dependent on the depth of the species in the water column. For the purpose of this  
556 study, we do not consider turbidity which also influences the light penetration in the water column. In this case,  
557 photosynthetically-active foraminifera living close to the surface should record microenvironment pH (thus  $\delta^{11}\text{B}$ )  
558 that is more sensitive to water depth changes. A deeper habitat reduces solar insolation, and as a consequence,  
559 may lower symbiont photosynthetic activity, possibly reducing pH in the foraminifera's micro-environment.  
560 This is supported by the significant trend observed between  $\Delta^{11}\text{B}$  and the calcification depth for *G. ruber* and *T.*  
561 *sacculifer* at our sites (Fig. S2), where microenvironment pH decreases with calcification depth. We observe a  
562 significant decrease in  $\delta^{11}\text{B}$  in the WEP for *T. sacculifer* (w/o sacc) compared to the other sites ( $p < 0.05$ ).  
563 Additionally, the  $\Delta^{11}\text{B}$  of *G. ruber*, *T. sacculifer* (w/o sacc and sacc) is significantly lower in the WEP compared  
564 to the other sites ( $p < 0.05$ ).

565 *T. sacculifer* has the potential to support more photosynthesis due to its higher symbiont density, and  
566 higher photosynthetic activity compared to other species, which may support higher symbiont/host interactions  
567 (Tagaki et al., 2019). These results would be consistent with a greater sensitivity of *T. sacculifer*'s  
568 photosynthetic activity with changes in insolation/water depth. To test if the low  $\delta^{11}\text{B}$  signature of *T. sacculifer*  
569 (w/o sacc) in the WEP is related to a decrease in light at greater water depth, we have independently calculated  
570 the calcification depth of the foraminifera based on various light insolation culture experiments (Jorgensen et al.,  
571 1985) and the microenvironment  $\Delta\text{pH}$  derived from our data (Fig. 8A and B). This exercise showed that the low  
572  $\delta^{11}\text{B}$  of *T. sacculifer* (w/o sacc) from the WEP can be explained by the reduced light environment due to a deeper  
573 depth habitat in the WEP (Fig. 8B). It can also be noted that this species exhibits the largest variation in  
574 symbiont density versus test size, suggesting that the low size fraction reported for the WEP (250–400  $\mu\text{m}$ )  
575 compared to the 300–400  $\mu\text{m}$  at the other sites could induce a change in photosynthetic activity and  $\delta^{11}\text{B}$ , but no  
576 weight per shell data were determined on the WEP samples to constrain if test size is significantly different  
577 across the different sites.

578 When the same approach of independently reconstructing calcification depth based on culture  
579 experiments is applied to *O. universa*, the boron data suggest a microenvironment pH of 0.10 to 0.20 lower than  
580 ambient seawater pH, which would be in line with the species living deeper than 50m (light compensation point  
581 (Ec), Rink et al., 1998), which is consistent with our calcification depth reconstructions. The low  $\delta^{11}\text{B}_{\text{carbonate}}$  of

582 *O. universa* compared to *T. sacculifer* for the similar calcification depth at some sites (e.g. FC-02a, WP07-a)  
583 might reflect differences in photosynthetic potential between the two species, which is supported by Tagaki et al.  
584 (2019) that observed that *O. universa* has a lower photosynthetic potential than *T. sacculifer*.

585 Microenvironment  $\Delta\text{pH}$  based on our  $\delta^{11}\text{B}_{\text{carbonate}}$  data were calculated for the rest of the species. We  
586 observed that microenvironment  $\Delta\text{pH}$  is higher in *T. sacculifer* > *G. ruber* > *T. sacculifer* (w/o sacc - WEP) > *O.*  
587 *universa*, *N. dutertrei*, *G. menardii*, *G. tumida* > *P. obliquiloculata*. These results are in line with the  
588 photosymbiosis findings from Tagaki et al., (2019). Also, the higher  $\delta^{11}\text{B}$  data from the West African upwelling  
589 published by Raitzsch et al., (2018) for *G. ruber* and *O. universa* may reflect a higher microenvironment pH due  
590 to a relatively shallow habitat, higher insolation and high rates of photosynthesis by symbionts. This could  
591 highlight a potential issue with calibration when applied to sites with different oceanic regimes as the  $\delta^{11}\text{B}$   
592 species-specific calibrations could be also location-specific for the mixed dweller species.

593 Microenvironment pH for *N. dutertrei*, *G. menardii* and *G. tumida* are similar to *O. universa* and  
594 suggest a threshold for a respiration-driven  $\delta^{11}\text{B}$  signature. This threshold can be induced by a change of  
595 photosynthetic activity at lower light intensity in deeper water and/or differences in symbiont density and/or by  
596 the type of symbionts at greater depth (non-dinoflagellate symbionts). We also note that *P. obliquiloculata*,  
597 which has the lowest symbiont density and photosynthetic activity (Takagi et al., 2019), has the lowest  
598 microenvironment pH compared to other deeper-dweller species, supporting our hypothesis that respiration can  
599 control microenvironment pH. The deep-dwelling species sensitivity of  $\delta^{11}\text{B}_{\text{carbonate}}$  to  $\delta^{11}\text{B}_{\text{borate}}$  with values close  
600 to unity might also be explained by a relatively stable respiration-driven microenvironments, as the deeper-  
601 dweller species do not experience large changes of insolation (e.g. photosynthesis), thereby making them a more  
602 direct recorder of environmental pH.

603

### 604 5.3 $\delta^{11}\text{B}$ sensitivity to $\delta^{11}\text{B}_{\text{borate}}$ and relationship with B/Ca signatures

605  $\delta^{11}\text{B}_{\text{carbonate}}$  and B/Ca data have shown to be sensitive to precipitation rate with at higher precipitation  
606 rate increasing  $\delta^{11}\text{B}_{\text{carbonate}}$  (Farmer et al., 2019) and B/Ca (Farmer et al., 2019; Gabitov et al., 2014; Kaczmarek  
607 et al., 2016; Mavromatis et al., 2015; Uchikawa et al., 2015). A recent study from Farmer et al, (2019) has  
608 proposed that in foraminifera at higher precipitation rates, more borate ion may be incorporated into the  
609 carbonate mineral, while more boric acid may be incorporated at lower precipitation rates. The authors also  
610 suggest this may explain low sensitivities of culture experiments.

611 When combining all literature data, *T. sacculifer* and *G. ruber* have sensitivities of  $\delta^{11}\text{B}_{\text{carbonate}}$  to  
612  $\delta^{11}\text{B}_{\text{borate}}$  of  $0.83 \pm 0.48$  and  $0.46 \pm 0.34$  respectively in line with previous literature and paleo- $\text{CO}_2$   
613 reconstructions. Also, if we only take into account our data, and the observation that the sensitivity of  $\delta^{11}\text{B}_{\text{carbonate}}$   
614 to  $\delta^{11}\text{B}_{\text{borate}}$  is not statistically different from unity for most of the species investigated, we can speculate that for  
615 these taxa, changes in precipitation rate and contributions of boric acid are not likely to be important. If  
616 considering only the data from this study, *G. ruber* ( $1.12 \pm 1.67$ ) and *T. sacculifer* ( $1.38 \pm 1.35$ ) present higher  
617 sensitivities of  $\delta^{11}\text{B}_{\text{carbonate}}$  to  $\delta^{11}\text{B}_{\text{borate}}$ . We can then again speculate that the observed high values for  $\delta^{11}\text{B}_{\text{carbonate}}$   
618 at high seawater pH can be due to higher precipitation rates. We note this could also be consistent with the  
619 higher sensitivity of B/Ca signatures in these two surface dwelling species to ambient  $[\text{B}(\text{OH})_4^-]/[\text{HCO}_3^-]$  relative  
620 to deeper-dwelling species. Those interspecific differences still remain to be explained, however, part of this  
621 variability is likely due to changes in the carbonate chemistry of the microenvironment resulting in changing



622 competition between borate and bicarbonate. A caveat is that we can not exclude specific biological processes,  
623 and that in taxa with a non respiration-driven microenvironment, changes in day/night calcification ratios also  
624 impacting observed values. As indicated by Farmer et al., (2019), studies of calcite precipitation rates in  
625 foraminifera may help to improve our understanding of the fundamental basis of boron-based proxies.

626

#### 627 **5.4 Evaluation of species for pH reconstructions and water depth pH reconstructions**

628 This data set allows us to reassess the utility of boron-based proxies for the carbonate system. The main  
629 aim of utilizing boron-based proxies relates to the reconstruction of past oceanic conditions, specifically pH and  
630 pCO<sub>2</sub>. Mixed-layer species (eg. *G. ruber* and *T. sacculifer*) are potential archives for atmospheric CO<sub>2</sub>  
631 reconstructions. Other species can shed light on other aspects of the carbon cycle including the physical and  
632 biological carbon pumps.

633 There are a few main inferences we can make. When integrated with published data, the sensitivities of  
634  $\delta^{11}\text{B}_{\text{carbonate}}$  to  $\delta^{11}\text{B}_{\text{borate}}$  for *G. ruber* and *T. sacculifer* are similar to previous studies (Martinez-Boti et al., 2015b;  
635 Raitzsch et al., 2018) which supports the fidelity of previous paleo-reconstructions that use published  
636 calibrations between  $\delta^{11}\text{B}_{\text{carbonate}}$  and  $\delta^{11}\text{B}_{\text{borate}}$ . The regression we have made for *G. ruber* supports a decrease in  
637  $\delta^{11}\text{B}_{\text{carbonate}}$  with decreasing size fractions (offset of -0.4 ‰, p>0.05) with the sensitivity of  $\delta^{11}\text{B}_{\text{carbonate}}$  to  $\delta^{11}\text{B}_{\text{borate}}$   
638 not being statistically different from higher size fraction (p<0.05). Our  $\delta^{11}\text{B}_{\text{carbonate}}$  data and the sensitivity to  
639  $\delta^{11}\text{B}_{\text{borate}}$  of *O. universa* supports previous data from Henehan et al., (2016). *N. dutertrei*  $\delta^{11}\text{B}_{\text{carbonate}}$  data span a  
640 large range of pH, allowing us to derive a robust calibration with  $\delta^{11}\text{B}_{\text{borate}}$ . Other species (*G. menardii*, *G.*  
641 *tumida* and *P. obliquiloculata*) need more data to better constrain their calibrations.

642 In order to derive accurate reconstructions of past ambient pH and pCO<sub>2</sub>, accurate species-specific  
643 calibrations need to be used that are constrained by core-tops or samples from similar types of settings (Fig. 9,  
644 10, S6). Lighter  $\delta^{11}\text{B}$  signatures in *T. sacculifer* (w/o sacc) are observed in the WEP, which may be explained by  
645 the deeper depth habitat for these taxa, where lower light levels might reduce symbiont photosynthetic activity.  
646 Also, we show that a correction is needed for *T. sacculifer* (w/o sacc) in the WEP in order to accurately  
647 reconstruct atmospheric CO<sub>2</sub>. When applying the calibrations n°2 and 4 to *T. sacculifer* and *G. ruber*  
648 (compilation of all data, Table 3) our data show more variability, especially for *G. ruber* which lead to the larger  
649 mismatch compared to *in situ* parameters. The greater divergence of reconstructed values from *in situ*  
650 measurements are observed at site WPO7-01 for both *T. sacculifer* (w/o sacc) and *G. ruber*. More data would be  
651 needed to determine a proper correction for both species, coretop study will be determinant for future downcore  
652 reconstructions, especially in the WEP.

653 We also find that for two species, the boron isotope-pH proxy is a relatively straightforward recorder of  
654 ambient pH, with sensitivities close to unity for *O. universa* and *N. dutertrei*. There is also promise in using  
655 multiple species in a sample from different hydrographic regimes to reconstruct vertical profiles of pH and  
656 pCO<sub>2</sub>. We are able to reproduce pH and pCO<sub>2</sub> profiles from multiple sites with different water column structures  
657 (Fig. 9) with those reconstructions within error of the *in situ* values, for most sites. In order to avoid circularity,  
658 to validate these calibrations, we recalculated ambient pH and pCO<sub>2</sub> by first excluding site-specific data and then  
659 recalculating species-specific calibrations, followed by application to each specific site. The comparison of the  
660 two methods does not show significant differences and validates the robustness of the calibrations (Fig. S5). We  
661 utilized the calibrations derived from our data for *G. ruber* (calibration n°1 and 2, Table 3), *T. sacculifer*

662 (calibration n°3 and 4, Table 3), *O. universa* (calibration n°8, Table 3), for *P. obliquiloculata* (calibration n°11,  
663 Table 3), and for *N. dutertrei*, *G. tumida* and *G. menardii* the calibration made on the compilation of the deep-  
664 dweller (calibration n°13, Table 3). Results are shown in Fig. 9 and evaluated in Fig. 10. For *G. menardii*, more  
665 data would be helpful to provide additional constraints. Results for *G. ruber* are the most scattered, potentially  
666 due to difference in test sizes (Henehan et al., 2013), or depth habitat, although we can not exclude  
667 undocumented diagenetic effects. Results reaffirm the importance of working with narrow size fractions  
668 (Henehan et al., 2013), the utilization of calibrations derived from the same size fraction or use of offsets to take  
669 into account this size fraction effect, and the importance of core-top studies before paleo-application.

670

## 671 **6. Conclusions and future implications**

672 Our study has extended the boron isotope proxy with data for new species and sites. The work supports  
673 previous work showing that depth habitats of foraminifera vary depending on the oceanic regime, and this can  
674 impact boron isotope signatures. Low  $\delta^{11}\text{B}$  values in the WEP compared to other regions for *T. sacculifer* (w/o  
675 sacc) may be explained by a reduction in microenvironment pH due to a deeper depth habitat associated with  
676 reduced irradiance and thus photosynthetic activity. Those results might also highlight a potential need for  
677 studying core-tops in order to establish what factors are important to accurately develop reconstructions in  
678 different areas.

679 The sensitivity of  $\delta^{11}\text{B}_{\text{carbonate}}$  to pH is in line with previously published data for *T. sacculifer*, *G. ruber*.  
680 The sensitivity of  $\delta^{11}\text{B}_{\text{carbonate}}$  to pH of *O. universa* (mixed-dweller), *N. dutertrei*, *G. menardii* and *G. tumida*  
681 (deep-dwellers) are similar but more data are needed to fully determine those sensitivities. The similarity of  
682 boron isotope calibrations for deep-dwelling taxa might be related to similar respiration-driven  
683 microenvironments.

684 Reconstruction of seawater pH and carbonate system parameters is achievable using foraminiferal  $\delta^{11}\text{B}$   
685 but additional core-top and down-core studies reconstructing depth profiles will be needed in order to further  
686 verify calibrations published to date. Past pH and  $\text{pCO}_2$  water depth profiles can potentially be created by  
687 utilizing multiple foraminiferal species in concert with taxon-specific calibrations for similar settings. This  
688 approach has much potential for enhancing our understanding of the past workings of the oceanic carbon cycle,  
689 and the biological pump.

690

691 **Author contribution**

692 R.E and A.T. wrote the proposals that funded the work. A.T. and F.C. provided the samples. M.G., S.M. and  
693 A.T. contributed to the experimental design. A.V. helped for sample preparation. M.G. and S.M contributed to  
694 developing the method of boron isotope analysis. M.G. performed the measurements with assistance from S.M.  
695 M.G conducted the data analysis. M.G. drafted the paper, which was edited by all authors. Interpretation was led  
696 by M.G., A.T., S.M. with input from R.E., A.V. and F.C.

697

698 **Competing interests**

699 The authors declare that they have no conflict of interest.

700

701 **Acknowledgments:**

702 The authors wish to thank Jesse Farmer for his valuable and detailed comments on the actual and a previous  
703 version of the manuscript. We wish to thank Michael Henehan for helpful discussion, comments on the  
704 manuscript and help with the code. We also want to thank the anonymous reviewer for helpful comments. Lea  
705 Bonnin for assistance with picking samples, the IODP repository for provision of samples, the Tripathi Laboratory  
706 (UCLA) for their technical support, Mervyn Greaves, Madeleine Bohlin (University of Cambridge) for technical  
707 support and use of laboratory space, Yoan Germain, Emmanuel Ponzevera and Oanez Lebeau for technical  
708 support and use of laboratory space in Brest, Jill Sutton for helpful conversation on the manuscript. Research is  
709 supported by DOE BES grant DE-FG02-13ER16402, by the International Research Chair Program that is funded  
710 by the French government (LabexMer ANR-10-LABX-19-01), and IAGC student research grant 2017.

711

712 **References**

- 713 Allen, K. A. and Hönisch, B.: The planktic foraminiferal B/Ca proxy for seawater carbonate chemistry, A critical  
714 evaluation, *Earth Planet. Sci. Lett.*, 345–348, 203–211, 2012.
- 715 Anagnostou, E., John, E., Edgar, K., Foster, G., Ridgwell, A., Inglis, G., Pancost, R., Lunt, D. and Pearson, P.,  
716 Changing atmospheric CO<sub>2</sub> concentration was the primary driver of early Cenozoic climate: *Nature* 533,  
717 380–384, 2016.
- 718 Anand, P., Elderfield, H. and Conte, M. H., Calibration of Mg/Ca thermometry in planktonic foraminifera from a  
719 sediment trap time series. *Paleoceanography* 18, 2003.
- 720 Anderson, O. R. and Bé, A.W. H.: The ultrastructure of a planktonic foraminifer, *Globigerinoides sacculifer*  
721 (Brady), and its symbiotic dinoflagellates: *J. Foramin. Res.*, 6, 1–21, 1976.
- 722 Axelsson, M. D., Rodushkin, I., Ingri, J. and Öhlander, B.: Multielemental analysis of Mn–Fe nodules by ICP-  
723 MS: optimisation of analytical method, *Analyst*, 127, 76–82, 2002.
- 724 Babila, T.L., Rosenthal, Y., Conte, M.H.: Evaluation of the biogeochemical controls on B/Ca of *Globigerinoides*  
725 *ruber* white from the Oceanic Flux Pro-gram, Bermuda, *Earth Planet. Sci. Lett.* 404, 67–76, 2014.
- 726 Barker, S., Greaves M. and Elderfield, H.: A study of cleaning procedures used for foraminiferal Mg/Ca  
727 paleothermometry, *Geochemistry, Geophys. Geosystems* 4, 1–20, 2003.
- 728 Bartoli, G., Hönisch, B. and Zeebe, R. E.: Atmospheric CO<sub>2</sub> decline during the Pliocene intensification of  
729 Northern Hemisphere glaciations, *Paleoceanography* 26, 1–14, 2011.
- 730 Bemis, B. E., Spero, H. J., Bijma, J. and Lea, D. W.: Reevaluation of the oxygen isotopic composition of  
731 planktonic foraminifera: Experimental results and revised paleotemperature equations, *Paleoceanography*  
732 13, 150–160, 1998.
- 733 Bemis, B. E., Spero, H. J. and Thunell, R. C.: Using species-specific paleotemperature equations with  
734 foraminifera: a case study in the Southern California Bight, *Mar. Micropaleontol.*, 46, 405–430, 2002.
- 735 Bijma, J., Faber Jr., W.W., Hemleben, C.: Temperature and salinity limits for growth and survival of some  
736 planktonic foraminifera in laboratory cultures, *J. Foraminiferal Res.* 20 (2), 95–116, 1990.
- 737 Bijma, J., Hönisch, B. and Zeebe, R. E.: Impact of the ocean carbonate chemistry on living foraminiferal shell  
738 weight: Comment on “Carbonate ion concentration in glacial-age deep waters of the Caribbean Sea” by W.  
739 S. Broecker and E. Clark, *Geochemistry, Geophys. Geosystems*, 3, 1–7, 2002.
- 740 Birch, H., Coxall, H. K., Pearson, P. N., Kroon, D. and O’Regan, M.: Planktonic foraminifera stable isotopes and  
741 water column structure, Disentangling ecological signals, *Mar. Micropaleontol.*, 101, 127–145, 2013.
- 742 Bird, C., Darling, K. F., Russell, A. D., Fehrenbacher, J. S., Davis, C. V., Free, A., & Ngwenya, B. T.: 16S  
743 rRNA gene metabarcoding and TEM reveals different ecological strategies within the genus  
744 *Neogloboquadrina* (planktonic foraminifer), *PloS one*, 13(1), 2018.
- 745 Boyer, T.P., Antonov, J. I., Baranova, O. K., Coleman, C., Garcia, H. E., Grodsky, A., Johnson, D. R., Locarnini,  
746 R. A., Mishonov, A. V., O’Brien, T.D., Paver, C.R., Reagan, J.R., Seidov, D., Smolyar, I. V., and Zweng,  
747 M. M.: *World Ocean Database*, NOAA Atlas NESDIS 72, S. Levitus, Ed., A. Mishonov, Technical Ed.,  
748 Silver Spring, MD, 209, 2013.
- 749 Boyle, E. A., Cadmium, zinc, copper, and barium in foraminifera tests, *Earth Planet. Sci. Lett.*, 53, 11–35, 1981.

- 750 Boyle, E. A., and L. D., Keigwin, Comparison of Atlantic and Pacific paleochemical records for the Last  
751 215,000 years: Changes in deep ocean circulation and chemical inventories, *Earth Planet. Sci. Lett.*, 76,  
752 135–150, 1985.
- 753 Branson, O., Kaczmarek, K., Redfern, S. A. T., Misra, S., Langer, G., Tyliszczak, T., Bijma, J. and Elderfield,  
754 H., The coordination and distribution of B in foraminiferal calcite, *Earth Planet. Sci. Lett.*, 416, 67–72,  
755 2015.
- 756 Catanzaro, E.J., Champion, C.E., Garner, A.L., Marinenko, G., Sappenfield, K.M. and Shields, W.R.: Boric  
757 Acid; Isotopic and Assay Standard Reference Materials, U.S. Natl. Bur. Stand. Spec., Publ. 260-17, 70p,  
758 1970.
- 759 Chalk, T. B., Hain, M. P., Foster, G. L., Rohling, E. J., Sexton, P. F., Badger, M. P. S., Cherry, S. G., Hasenfratz,  
760 A. P., Haug, G. H., Jaccard, S. L., Martínez-García, A., Pälike, H., Pancost, R. D. and Wilson, P. A.,  
761 Causes of ice age intensification across the Mid-Pleistocene Transition, *Proc. Natl. Acad. Sci.*, 114,  
762 13114–13119, 2017.
- 763 Coadic, R., Bassinot, F., Dissard, D., Douville, E., Greaves, M. and Michel, E., A core-top study of dissolution  
764 effect on B/Ca in Globigerinoides sacculifer from the tropical Atlantic: Potential bias for paleo-  
765 reconstruction of seawater carbonate chemistry, *Geochemistry, Geophys. Geosystems* 14, 1053–1068,  
766 2013.
- 767 de Nooijer, L. J., Spero, H. J., Erez, J., Bijma, J. and Reichart, G. J., Biomineralization in perforate foraminifera.  
768 *Earth-Science Rev.*, 135, 48–58, 2014.
- 769 Dekens, P. S., Lea, D. W., Pak, D. K. and Spero, H. J., Core top calibration of Mg/Ca in tropical foraminifera,  
770 Refining paleotemperature estimation, *Geochemistry, Geophys. Geosystems* 3, 1–29, 2002.
- 771 Deuser, W.G., Ross, E.H., Hemleben, Ch., Spindler, M., Seasonal changes in species composition, numbers,  
772 mass, size, and isotopic composition of planktonic foraminifera settling into the deep Sargasso Sea,  
773 *Palaeogeogr., Palaeoclimat., Palaeoecol.*, 33:103-127, 1981.
- 774 Deuser, W. G. and Ross, E. H., Seasonally abundant planktonic foraminifera of the Sargasso Sea; succession,  
775 deep-water fluxes, isotopic compositions, and paleoceanographic implications, *J. Foraminifer. Res.* 19,  
776 268–293, 1989.
- 777 Dickson, A. G., Thermodynamics of the dissociation of boric acid in synthetic seawater from 273.15 to 318.15  
778 K., *Deep Sea Res., Part A, Oceanogr. Res. Pap.* 37, 755–766, 1990.
- 779 Dickson, A.G., Millero, F.J., A comparison of the equilibrium constants for the dissociation of carbonic acid in  
780 seawater media, *Deep-Sea Res.*, 34, 1733–1743, 1987.
- 781 Douville, E., Paterne, M., Cabioch, G., Louvat, P., Gaillardet, J., Juillet-Leclerc, A. and Ayliffe, L., Abrupt sea  
782 surface pH change at the end of the Younger Dryas in the central sub-equatorial Pacific inferred from  
783 boron isotope abundance in corals (*Porites*), *Biogeosciences* 7, 2445–2459, 2010.
- 784 Duguay, L.E., Comparative laboratory and field studies on calcification and carbon fixation in foraminiferal-  
785 algal associations, *Journal of Foraminiferal Research* 13, 252-261, 1983.
- 786 Duplessy, J., Labeyrie, L., Juilletleclerc, A., Maitre, F., Duprat, J. and Sarnthein, M.: Surface salinity  
787 reconstruction of the north-atlantic ocean during the last glacial maximum, *Oceanol. Acta*, 14, 311–324,  
788 1991.
- 789 Elderfield, H., Yu, J., Anand, P., Kiefer, T. and Nyland, B., Calibrations for benthic foraminiferal Mg/Ca  
790 paleothermometry and the carbonate ion hypothesis, *Earth Planet. Sci. Lett.*, 250, 633–649., 2006.

- 791 Elderfield, H. and Granssen, G., Past temperatures and O18 of surface ocean waters inferred from foraminiferal  
792 Mg/Ca ratios, *Nature* 405, 442–445, 2000.
- 793 Erez J., Calcification Rates, Photosynthesis and Light in Planktonic Foraminifera. In: Westbroek P., de Jong  
794 E.W. (eds) *Biom mineralization and Biological Metal Accumulation*. Springer, Dordrecht, 1983.
- 795 Erez, J., The Source of Ions for Biom mineralization in Foraminifera and Their Implications for Paleoceanographic  
796 Proxies, *Rev. Mineral. Geochemistry*, 54, 115–149, 2003.
- 797 Fairbanks, R. G. and Wiebe, P. H.: Foraminifera and Chlorophyll Maximum: Vertical Distribution, Seasonal  
798 Succession, and Paleoceanographic Significance, *Science*, 209, 1524–1526, 1980.
- 799 Fairbanks, R. G., Sverdløve, M., Free, R., Wiebe, P. H. and Bé, A. W. H.: Vertical distribution and isotopic  
800 fractionation of living planktonic foraminifera from the Panama Basin, *Nature*, 298, 841–844, 1982.
- 801 Farmer, E. C., Kaplan, A., de Menocal, P. B. and Lynch-Stieglitz, J., Corroborating ecological depth preferences  
802 of planktonic foraminifera in the tropical Atlantic with the stable oxygen isotope ratios of core top  
803 specimens, *Paleoceanography*, 22, 1–14, 2007.
- 804 Feely, R., Impact of Anthropogenic CO<sub>2</sub> on the CaCO<sub>3</sub> System in the Oceans, *Science*, 305, 362–366, 2004.
- 805 Ferguson, J. E., Henderson, G. M., Kucera, M. and Rickaby, R. E. M.: Systematic change of foraminiferal  
806 Mg/Ca ratios across a strong salinity gradient, *Earth Planet. Sci. Lett.*, 265, 153–166, 2008.
- 807 Foster, G. L., Seawater pH, pCO<sub>2</sub> and [CO<sub>3</sub><sup>2-</sup>] variations in the Caribbean Sea over the last 130 kyr: A boron  
808 isotope and B/Ca study of planktic foraminifera, *Earth Planet. Sci. Lett.*, 271, 254–266, 2008.
- 809 Foster, G. L. and Sexton, P. F.: Enhanced carbon dioxide outgassing from the eastern equatorial Atlantic during  
810 the last glacial, *Geology*, 42, 1003–1006, 2014.
- 811 Foster, G. L., Lear, C. H. and Rae, J. W. B., The evolution of pCO<sub>2</sub>, ice volume and climate during the middle  
812 Miocene, *Earth Planet. Sci. Lett.*, 341–344, 243–254, 2012.
- 813 Foster, G. L. and Rae, J. W. B., Reconstructing Ocean pH with Boron Isotopes in Foraminifera, *Annu. Rev.*  
814 *Earth Planet. Sci.*, 44, 207–237, 2016.
- 815 Gabitov, R. I., Rollion-bard, C., Tripathi, A. and Sadekov, A., In situ study of boron partitioning between calcite  
816 and fluid at different crystal growth rates, *Geochim. Cosmochim. Acta*, 137, 81–92, 2014.
- 817 Gaillardet, J., Lemarchand, D., Göpel, C. and Manhès, G., Evaporation and Sublimation of Boric Acid :  
818 Application for Boron Purification from Organic Rich Solutions, *Geostand. Newsl.*, 25, 67–75, 2001.
- 819 Gast, R. J. and Caron D. A., Photosymbiotic associations in planktonic foraminifera and radiolaria, 1–7, 2001.
- 820 Gastrich, M.D., Ultrastructure of a new intracellular symbiotic alga found within planktonic foraminifera,  
821 *Journal of Phycology* 23, 623–632, 1988.
- 822 Gattuso, J.P. and Hansson, L., *Ocean acidification*, Oxford University Press, 2011.
- 823 Gutjahr, M., Bordier, L., Douville, E., Farmer, J., Foster, G. L., Hathorne, E., Hönish, B., Lemarchand, D.,  
824 Louvat, P., McCulloch, M., Noireaux, J., Pallavicini, N., Rodushkin, I., Roux, P., Stewart, J., Thil, F. You,  
825 C.F., Boron Isotope Intercomparison Project (BIIP): Development of a new carbonate standard for stable  
826 isotopic analyses. In EGU general assembly conference abstracts, Vol. 16, (2014).
- 827 Hallock P., *Algal Symbiosis : A Mathematical Analysis Marine Biology* 62, 249–255, 1981b.

- 828 Hemming, N. G. and Hanson, G. N. Boron isotopic composition and concentration in modern marine carbonates,  
829 *Geochim. Cosmochim. Acta*, 56, 537–543, 1992.
- 830 Hendry, K.R., Rickaby, R.E.M., Meredith, M.P., Elderfield, H., Controls on stable isotope and trace metal  
831 uptake in *Neogloboquadrina pachyderma* (sinistral) from an Antarctic sea-ice environment. *Earth Planet.*  
832 *Sci. Lett.* 278, 67–77, 2009.
- 833 Henehan, M. J., Foster, G. L., Bostock, H. C., Greenop, R., Marshall, B. J. and Wilson, P. A., A new boron  
834 isotope-pH calibration for *Orbulina universa*, with implications for understanding and accounting for ‘vital  
835 effects’, *Earth Planet. Sci. Lett.*, 454, 282–292, 2016.
- 836 Henehan, M. J., Foster, G. L., Rae, J. W. B., Prentice, K. C., Erez, J., Bostock, H. C., Marshall, B. J. and Wilson,  
837 P. A., Evaluating the utility of B/Ca ratios in planktic foraminifera as a proxy for the carbonate system: A  
838 case study of *Globigerinoides ruber*, *Geochemistry, Geophys. Geosystems* 16, 1052–1069, 2015.
- 839 Henehan, M. J., Rae, J. W. B., Foster, G. L., Erez, J., Prentice, K. C., Kucera, M., Bostock, H. C., Martínez-Botí,  
840 M. A., Milton, J. A., Wilson, P. A., Marshall, B. J. and Elliott, T., Calibration of the boron isotope proxy in  
841 the planktonic foraminifera *Globigerinoides ruber* for use in palaeo-CO<sub>2</sub> reconstruction, *Earth Planet. Sci.*  
842 *Lett.* 364, 111–122, 2013.
- 843 Holcomb, M., Decarlo, T. M., Schoepf, V., Dissard, D., Tanaka, K. and McCulloch, M.: Cleaning and pre-  
844 treatment procedures for biogenic and synthetic calcium carbonate powders for determination of elemental  
845 and boron isotopic compositions, *Chem. Geol.*, 398, 11–21, 2015.
- 846 Hönisch, B., Hemming, N. G., Archer, D., Siddall, M. and McManus, J. F., Atmospheric Carbon Dioxide  
847 Concentration Across the Mid-Pleistocene Transition, *Science*, 324, 1551–1554, 2009.
- 848 Hönisch, B., Bijma, J., Russell, A. D., Spero, H. J., Palmer, M. R., Zeebe, R. E. and Eisenhauer, A., The  
849 influence of symbiotic photosynthesis on the boron isotopic composition of foraminifera shells, *Mar.*  
850 *Micropaleontol.*, 49, 87–96, 2003.
- 851 Hönisch, B. and Hemming, N. G., Ground-truthing the boron isotope-paleo-pH proxy in planktonic foraminifera  
852 shells: Partial dissolution and shell size effects, *Paleoceanography* 19, 1–13, 2004.
- 853 Hönisch, B., Bickert, T. and Hemming, N. G., Modern and Pleistocene boron isotope composition of the benthic  
854 foraminifer *Cibicides wuellerstorfi*, *Earth Planet. Sci. Lett.*, 272, 309–318, 2008.
- 855 Howes, E. L., Kaczmarek, K., Raitzsch, M., Mewes, A., Bijma, N., Horn, I., Misra, S., Gattuso, J. P. and Bijma,  
856 J., Decoupled carbonate chemistry controls on the incorporation of boron into *Orbulina universa*,  
857 *Biogeosciences*, 14, 415–430, 2017.
- 858 IPCC: Climate Change 2014 - The Physical Science Basis, edited by Intergovernmental Panel on Climate  
859 Change, Cambridge University Press, Cambridge., 2014.
- 860 Jørgensen, B. B., Erez, J., Revsbech, P. and Cohen, Y., Symbiotic photosynthesis in a planktonic foraminifera,  
861 *Globigerinoides sacculifer* (Brady), studied with microelectrodes, *Limnol. Oceanogr.*, 30, 1253–1267  
862 1985.
- 863 Kaczmarek, K., Nehrke, G., Misra, S., Bijma, J. and Elderfield, H., Investigating the effects of growth rate and  
864 temperature on the B/Ca ratio and  $\delta^{11}\text{B}$  during inorganic calcite formation, *Chem. Geol.*, 421, 81–92,  
865 2016.
- 866 Kemle-von Mücke S. and Oberhänsli H., The Distribution of Living Planktic Foraminifera in Relation to  
867 Southeast Atlantic Oceanography, *Use Proxies Paleocyanogr.*, 91–115, 1999.
- 868 Key, R.M., A global ocean carbon climatology: Results from Global Data Analysis Project (GLODAP), *Global*  
869 *Biogeochem. Cycles*, 18, GB4031, 2004.

- 870 Kim, S.T. and O'Neil, J. R., Equilibrium and nonequilibrium oxygen isotope effects in synthetic carbonates,  
871 *Geochim. Cosmochim. Acta*, 61, 3461–3475, 1997.
- 872 Klochko, K., Cody, G. D., Tossell, J. A., Dera, P. and Kaufman, A. J., Re-evaluating boron speciation in  
873 biogenic calcite and aragonite using  $^{11}\text{B}$  MAS NMR, *Geochim. Cosmochim. Acta*, 73, 1890–1900, 2009.
- 874 Klochko, K., Kaufman, A. J., Yao, W., Byrne, R. H. and Tossell, J. A., Experimental measurement of boron  
875 isotope fractionation in seawater, *Earth Planet. Sci. Lett.*, 248, 276–285, 2006.
- 876 Köhler-Rink, S. and Kühl, M., Microsensor studies of photosynthesis and respiration in larger symbiotic  
877 foraminifera. I. The physico-chemical microenvironment of *Marginopora vertebralis*, *Amphistegina*  
878 *lobifera* and *Amphisorus hemrichii*, *Mar. Biol.*, 137, 473–486, 2000.
- 879 Köhler-Rink, S. and Kühl, M., Microsensor studies of photosynthesis and respiration in the larger symbiont  
880 bearing foraminifera *Amphistegina lobifera*, and *Amphisorus hemprichii*, *Ophelia*, 55, 111–122, 2001.
- 881 Lea, D. W., Pak, D. K. and Spero, H. J., Climate impact of late quaternary equatorial Pacific sea surface  
882 temperature variations, *Science*, 289, 1719–1724, 2000.
- 883 Lemarchand, D., Gaillardet, J., Lewin, A. and Allègre, C. J., Boron isotope systematics in large rivers:  
884 Implications for the marine boron budget and paleo-pH reconstruction over the Cenozoic, *Chem. Geol.*,  
885 190, 123–14, 2002.
- 886 Liu, Y., Liu, W., Peng, Z., Xiao, Y., Wei, G., Sun, W., He, J., Liu, G. and Chou, C.L., Instability of seawater pH  
887 in the South China Sea during the mid-late Holocene: Evidence from boron isotopic composition of corals,  
888 *Geochim. Cosmochim. Acta*, 73, 1264–1272, 2009.
- 889 Lloyd, N. S., Sadekov, A. Y. and Misra, S., Application of 1013ohm Faraday cup current amplifiers for boron  
890 isotopic analyses by solution mode and laser ablation multicollector inductively coupled plasma mass  
891 spectrometry, *Rapid Commun. Mass Spectrom.*, 32, 9–18, 2018.
- 892 Martínez-Botí, M. A., Foster, G. L., Chalk, T. B., Rohling, E. J., Sexton, P. F., Lunt, D. J., Pancost, R. D.,  
893 Badger, M. P. S. and Schmidt, D. N., Plio-Pleistocene climate sensitivity evaluated using high-resolution  
894  $\text{CO}_2$  records, *Nature*, 518, 49–54, 2015a.
- 895 Martínez-Botí M. A., Marino G., Foster G. L., Ziveri P., Henahan M. J., Rae J. W. B., Mortyn P. G. and Vance  
896 D., Boron isotope evidence for oceanic carbon dioxide leakage during the last deglaciation. *Nature*, 518,  
897 219–222, 2015b.
- 898 Martínez-Botí, M. A., Mortyn, P. G., Schmidt, D. N., Vance, D. and Field, D. B., Mg/Ca in foraminifera from  
899 plankton tows: Evaluation of proxy controls and comparison with core tops, *Earth Planet. Sci. Lett.*, 307,  
900 113–125, 2011.
- 901 Mavromatis, V., Montouillout, V., Noireaux, J., Gaillardet, J. and Schott, J., Characterization of boron  
902 incorporation and speciation in calcite and aragonite from co-precipitation experiments under controlled  
903 pH, temperature and precipitation rate, *Geochim. Cosmochim. Acta*, 150, 299–313, 2015.
- 904 McCulloch, M. T., D'Olivo, J. P., Falter, J. L., Georgiou, L., Holcomb, M., Montagna, P. and Trotter, J. A.,  
905 Boron Isotopic Systematics in Scleractinian Corals and the Role of pH Up-regulation, *Boron Isot. Adv.*  
906 *Isot. Geochemistry*, 2018.
- 907 Misra, S., Greaves, M., Owen, R., Kerr, J., Elmore, A. C. and Elderfield, H.: Determination of B/Ca of natural  
908 carbonates by HR-ICP-MS, *Geochemistry, Geophys. Geosystems*, 15, 1617–1628, 2014a.
- 909 Misra, S., Owen, R., Kerr, J., Greaves, M. and Elderfield, H., Determination of  $\delta^{11}\text{B}$  by HR-ICP-MS from mass  
910 limited samples: Application to natural carbonates and water samples, *Geochim. Cosmochim. Acta*, 140,  
911 531–552, 2014b.



- 912 Mortyn, P. G. and Charles, C. D., Planktonic foraminiferal depth habitat and  $\delta^{18}\text{O}$  calibrations: Plankton tow  
913 results from the Atlantic sector of the Southern Ocean, *Paleoceanography*, 18, 2003.
- 914 Mulitza, S., Boltovskoy, D., Donner, B., Meggers, H., Paul, A. and Wefer, G., Temperature: $\delta^{18}\text{O}$  relationships  
915 of planktonic foraminifera collected from surface waters, *Palaeogeogr. Palaeoclimatol. Palaeoecol.*, 202,  
916 143–152, 2003.
- 917 Ni, Y., Foster, G. L., Bailey, T., Elliott, T., Schmidt, D. N., Pearson, P., Haley, B. and Coath, C., A core top  
918 assessment of proxies for the ocean carbonate system in surface-dwelling foraminifers, *Paleoceanography*  
919 22, 2007.
- 920 Nir, O., Vengosh, A., Harkness, J. S., Dwyer, G. S. and Lahav, O., Direct measurement of the boron isotope  
921 fractionation factor: Reducing the uncertainty in reconstructing ocean paleo-pH, *Earth Planet. Sci. Lett.*,  
922 414, 1–5, 2015.
- 923 Noireaux, J., Mavromatis, V., Gaillardet, J., Schott, J., Montouillout, V., Louvat, P., Rollion-Bard, C. and  
924 Neuville, D. R., Crystallographic control on the boron isotope paleo-pH proxy, *Earth Planet. Sci. Lett.*,  
925 430, 398–407, 2015.
- 926 Orr, J. C., Fabry, V. J., Aumont, O., Bopp, L., Doney, S. C., Feely, R. A., Gnanadesikan, A., Gruber, N., Ishida,  
927 A., Joos, F., Key, R. M., Lindsay, K., Maier-Reimer, E., Matear, R., Monfray, P., Mouchet, A., Najjar, R.  
928 G., Plattner, G. K., Rodgers, K. B., Sabine, C. L., Sarmiento, J. L., Schlitzer, R., Slater, R. D., Totterdell, I.  
929 J., Weirig, M. F., Yamanaka, Y. and Yool, A., Anthropogenic ocean acidification over the twenty-first  
930 century and its impact on calcifying organisms, *Nature*, 437, 681–686, 2005.
- 931 Pagani, M., Marked Decline in Atmospheric Carbon Dioxide Concentrations During the Paleogene, *Science*,  
932 309, 600–603, 2005.
- 933 Palmer, M. R., Pearson, P. N. and Cobb, S. J., Reconstructing Past Ocean pH-Depth Profiles, *Science*, 282,  
934 1468–1471, 1998.
- 935 Pearson, P. N. and Palmer, M. R., Middle Eocene seawater pH and atmospheric carbon dioxide concentrations,  
936 *Science*, 284, 1824–1826, 1999.
- 937 Peeters, F. J. C. and Brummer, G.J. a., The seasonal and vertical distribution of living planktic foraminifera in  
938 the NW Arabian Sea, *Geol. Soc. London, Spec. Publ.*, 195, 463–497, 2002.
- 939 Quintana Krupinski, N. B., Russell, A. D., Pak, D. K. and Paytan, A., Core-top calibration of B/Ca in Pacific  
940 Ocean *Neoglobobulimina incompacta* and *Globigerina bulloides* as a surface water carbonate system proxy,  
941 *Earth Planet. Sci. Lett.*, 466, 139–151, 2017.
- 942 Rae, J.W.B.: Boron Isotopes in Foraminifera: Systematics, Biomineralisation, and  $\text{CO}_2$  Reconstruction. In,  
943 Marschall, H., Foster, G. (eds), *Boron Isotopes. Advances in Isotope Geochemistry*. Springer, Cham, 2018.
- 944 Rae, J. W. B., Foster, G. L., Schmidt, D. N. and Elliott, T., Boron isotopes and B/Ca in benthic foraminifera:  
945 Proxies for the deep ocean carbonate system, *Earth Planet. Sci. Lett.*, 302, 403–413, 2011.
- 946 Raitzsch, M., Bijma, J., Benthien, A., Richter, K.-U., Steinhofel, G. and Kučera, M., Boron isotope-based  
947 seasonal paleo-pH reconstruction for the Southeast Atlantic – A multispecies approach using habitat  
948 preference of planktonic foraminifera, *Earth Planet. Sci. Lett.*, 487, 138–150, 2018.
- 949 Ravelo, A. C. and Fairbanks, R. G., Oxygen isotopic composition of multiple species of planktonic foraminifera:  
950 recorder of the modern photic zone temperature gradient, *Palaeogeogr. Palaeoclimatol. Palaeoecol.*, 7,  
951 815–831, 1992.

- 952 Rebotim, A., Voelker, A. H. L., Jonkers, L., Waniek, J. J., Meggers, H., Schiebel, R., Fraile, I., Schulz, M., and  
 953 Kucera, M., Factors controlling the depth habitat of planktonic foraminifera in the subtropical eastern  
 954 North Atlantic, *Biogeosciences*, 14, 827–859, <https://doi.org/10.5194/bg-14-827-2017>, 2017.
- 955 Regenberg, M., Steph, S., Nürnberg, D., Tiedemann, R. and Garbe-Schönberg, D.: Calibrating Mg/Ca ratios of  
 956 multiple planktonic foraminiferal species with  $\delta^{18}\text{O}$ -calcification temperatures, *Paleothermometry for the*  
 957 *upper water column*, *Earth Planet. Sci. Lett.*, 278, 324–336, 2009.
- 958 Rickaby, R. E. M. and Halloran, P., Cool La Nina During the Warmth of the Pliocene?, *Science*, 307, 1948–  
 959 1952, 2005.
- 960 Ries, J. B., Cohen, A. L. and McCorkle, D. C., Marine calcifiers exhibit mixed responses to CO<sub>2</sub>-induced ocean  
 961 acidification, *Geology*, 37, 1131–1134, 2009.
- 962 Rink, S., Kühl, M., Bijma, J. and Spero, H. J., Microsensor studies of photosynthesis and respiration in the  
 963 symbiotic foraminifer *Orbulina universa*, *Mar. Biol.*, 131, 583–595, 1998.
- 964 Rollion-Bard, C. and Erez, J., Intra-shell boron isotope ratios in the symbiont-bearing benthic foraminiferan  
 965 *Amphistegina lobifera*: Implications for  $\delta^{11}\text{B}$  vital effects and paleo-pH reconstructions, *Geochim.*  
 966 *Cosmochim. Acta*, 74, 1530–1536, 2010.
- 967 Rostek, F., Ruhland, G., Bassinot, F. C., Muller, P. J., Labeyrie, L. D., Lancelot, Y. and Bard, E., Reconstructing  
 968 Sea-Surface Temperature and Salinity Using  $\delta^{18}\text{O}$  and Alkenone Records, *Nature*, 364, 319–321, 1993.
- 969 Russell, A. D., Hönisch, B., Spero, H. J. and Lea, D. W., Effects of seawater carbonate ion concentration and  
 970 temperature on shell U, Mg, and Sr in cultured planktonic foraminifera, *Geochim. Cosmochim. Acta*, 68,  
 971 4347–4361, 2004.
- 972 Sanyal, A., Bijma, J., Spero, H. J. and Lea, D. W., Empirical relationship between pH and the boron isotopic  
 973 composition of *Globigerinoides sacculifer*: Implications for the boron isotopes paleo-pH proxy,  
 974 *Paleoceanography*, 16, 515–519, 2001.
- 975 Sanyal, A., Hemming, N. G., Broecker, W. S., Lea, D. W., Spero, H. J., & Hanson, G. N. Oceanic pH control on  
 976 the boron isotopic composition of foraminifera: evidence from culture experiments, *Paleoceanography*,  
 977 11(5), 513-517, 1996.
- 978 Shaked, Y. and de Vargas, C., Pelagic photosymbiosis: rDNA assessment of diversity and evolution of  
 979 dinoflagellate symbionts and planktonic foraminiferal hosts, *Marine Ecology Progress Serie*, 325, 59–71,  
 980 2006.
- 981 Schmidt, G. A. and Mulitza, S., Global calibration of ecological models for planktic foraminifera from core-top  
 982 carbonate oxygen-18, *Mar. Micropaleontol.*, 44, 125–140, 2002.
- 983 Seki, O., Foster, G. L., Schmidt, D. N., Mackensen, A., Kawamura, K. and Pancost, R. D., Alkenone and boron-  
 984 based Pliocene pCO<sub>2</sub> records, *Earth Planet. Sci. Lett.*, 292, 201–211, 2010.
- 985 Shirayama, Y., Effect of increased atmospheric CO<sub>2</sub> on shallow water marine benthos, *J. Geophys. Res.*, 110,  
 986 C09S08, 2005.
- 987 Sime, N. G., De La Rocha, C. L. and Galy, A., Negligible temperature dependence of calcium isotope  
 988 fractionation in 12 species of planktonic foraminifera, *Earth Planet. Sci. Lett.*, 232, 51–66, 2005.
- 989 Spero H. J., Symbiosis in the planktonic foraminifer, *Orbulina universa*, and the isolation of its symbiotic  
 990 dinoflagellate, *Gymnodinium beii* sp. nov., *J. Phycol.* 23, 307-317, 1987.
- 991 Sutton, J. N., Liu, Y. W., Ries, J. B., Guillemeric, M., Ponzevera, E. and Eagle, R. A.,  $\delta^{11}\text{B}$  as monitor of  
 992 calcification site pH in divergent marine calcifying organisms, *Biogeosciences*, 15, 1447–1467, 2018.

- 993 Takagi H., Kimoto K., Fujiki T., Saito H., Schmidt C. and Kucera M., Characterizing photosymbiosis in modern  
994 planktonic foraminifera, *biogeosciences*, 3377–3396, 2019.
- 995 Thomson, J., Brown, L., Nixon, S., Cook, G. T. and MacKenzie, A. B., Bioturbation and Holocene sediment  
996 accumulation fluxes in the north-east Atlantic Ocean (Benthic Boundary Layer experiment sites), *Mar.*  
997 *Geol.*, 169, 21–39, 2000.
- 998 Tripathi, A., Deep-Sea Temperature and Circulation Changes at the Paleocene-Eocene Thermal Maximum.  
999 *Science*, 308, 1894–1898, 2005.
- 1000 Tripathi, A. K., Roberts, C. D. and Eagle, R. A., Coupling of CO<sub>2</sub> and Ice Sheet Stability Over Major Climate  
1001 Transitions of the Last 20 Million Years, *Science*, 326, 1394–1397, 2009.
- 1002 Tripathi, A. K., Roberts, C. D., Eagle, R. A. and Li, G., A 20 million year record of planktic foraminiferal B/Ca  
1003 ratios: Systematics and uncertainties in pCO<sub>2</sub> reconstructions, *Geochim. Cosmochim. Acta*, 75, 2582–  
1004 2610, 2011.
- 1005 Uchikawa, J., Penman, D. E., Zachos, J. C. and Zeebe, R. E., Experimental evidence for kinetic effects on B/Ca  
1006 in synthetic calcite: Implications for potential B(OH)<sub>4</sub><sup>-</sup> and B(OH)<sub>3</sub> incorporation, *Geochim. Cosmochim.*  
1007 *Acta*, 150, 171–191, 2015.
- 1008 Urey, H.C., Lowenstam, H.A., Epstein, S. & McKinney, C.R.: Measurement of paleo-temperature and  
1009 temperatures of the upper cretaceous of England, Denmark, and the southeastern United-States. *Geol. Soc.*  
1010 *Am. Bull.*, 62, 399-416, 1951.
- 1011 Wang, B.-S., You, C.-F., Huang, K.-F., Wu, S.-F., Aggarwal, S. K., Chung, C.-H. and Lin, P.-Y., Direct  
1012 separation of boron from Na- and Ca-rich matrices by sublimation for stable isotope measurement by MC-  
1013 ICP-MS, *Talanta*, 82, 1378–1384, 2010.
- 1014 Wang, G., Cao, W., Yang, D. and Xu, D., Variation in downwelling diffuse attenuation coefficient in the  
1015 northern South China Sea, *Chinese J. Oceanol. Limnol.*, 26, 323–333, 2008.
- 1016 Weare, B. C., Strub, P. T. and Samuel, M. D., Annual Mean Surface Heat Fluxes in the Tropical Pacific Ocean,  
1017 *J. Phys. Oceanogr.*, 11, 705–717, 1981.
- 1018 Wei, G., McCulloch, M. T., Mortimer, G., Deng, W. and Xie, L., Evidence for ocean acidification in the Great  
1019 Barrier Reef of Australia, *Geochim. Cosmochim. Acta*, 73, 2332–2346, 2009.
- 1020 Wilson, D. J., Piotrowski, A. M., Galy, A. and McCave, I. N., A boundary exchange influence on deglacial  
1021 neodymium isotope records from the deep western Indian Ocean, *Earth Planet. Sci. Lett.*, 341–344, 35–47,  
1022 2012.
- 1023 Wolf-Gladrow, D. A., Riebesell, U., Burkhardt, S. and Buma, J., Direct effects of CO<sub>2</sub> concentration on growth  
1024 and isotopic composition of marine plankton, *Tellus B Chem. Phys. Meteorol.*, 51, 461–476, 1999.
- 1025 Yu, J., Menviel, L., Jin, Z. D., Thornalley, D. J. R., Barker, S., Marino, G., Rohling, E. J., Cai, Y., Zhang, F.,  
1026 Wang, X., Dai, Y., Chen, P. and Broecker, W. S., Sequestration of carbon in the deep Atlantic during the  
1027 last glaciation, *Nat. Geosci.*, 9, 319–324, 2016.
- 1028 Yu, J., Thornalley, D. J. R., Rae, J. W. B. and McCave, N. I., Calibration and application of B/Ca, Cd/Ca, and  $\delta$   
1029  $^{11}\text{B}$  in *Neogloboquadrina pachyderma* (sinistral) to constrain CO<sub>2</sub> uptake in the subpolar North Atlantic  
1030 during the last deglaciation, *Paleoceanography*, 28, 237–252, 2013.
- 1031 Yu, J., Foster, G. L., Elderfield, H., Broecker, W. S. and Clark, E., An evaluation of benthic foraminiferal B/Ca  
1032 and  $\delta^{11}\text{B}$  for deep ocean carbonate ion and pH reconstructions, *Earth Planet. Sci. Lett.*, 293, 114–120, 20,  
1033 2010.

- 1034 Yu, J., Elderfield, H., Hönisch, B., B/Ca in planktonic foraminifera as a proxy for surface seawater pH.  
1035 *Paleoceanography* 22, PA2202, 2007.
- 1036 Yu, J., Day, J., Greaves, M. and Elderfield, H., Determination of multiple element/calcium ratios in foraminiferal  
1037 calcite by quadrupole ICP-MS, *Geochemistry, Geophys. Geosystems* 6, 2005.
- 1038 Zeebe, R. E. and Wolf-Gladrow, D., *CO<sub>2</sub> in Seawater: Equilibrium, Kinetics, Isotopes* Elsevier Oceanography  
1039 Series 65, Amsterdam, 2001.
- 1040 Zeebe, R. E., Wolf-Gladrow, D. A., Bijma, J. and Hönisch, B., Vital effects in foraminifera do not compromise  
1041 the use of  $\delta^{11}\text{B}$  as a paleo- pH indicator: Evidence from modeling, *Paleoceanography*, 18, 2003.

1042 **Figure caption**

1043

1044 **Figure 1:** Reactions governing dissolved inorganic carbon equilibria.

1045

1046 **Figure 2:** (A) Speciation of  $B(OH)_3$  and  $B(OH)_4^-$  as function of seawater pH (total scale), (B)  $\delta^{11}B$  of dissolved  
1047 inorganic boron species as a function of seawater pH, (C) sensitivity of  $\delta^{11}B$  of  $B(OH)_4^-$  for a pH ranging from  
1048 7.6 to 8.4.  $T=25^\circ C$ ,  $S=35$ ,  $\delta^{11}B=39.61$  ‰ (Foster et al., 2010), dissociation constant  $\alpha = 1.0272$  (Klochko et al.,  
1049 2006).

1050

1051 **Figure 3:** Map showing locations of the core-tops used in this study (white diamonds). Red open circles  
1052 represent the sites used for *in situ* carbonate parameters from GLODAP database (Key et al., 2004).

1053

1054 **Figure 4:** Pre-industrial data versus depth for the sites used in this study. The figure shows seasonal  
1055 temperatures (extracted from World Ocean Database 2013), density anomaly ( $kg/m^3$ ), pre-industrial pH and pre-  
1056 industrial  $\delta^{11}B$  of  $H_4BO_4^-$  (calculated from the GLODAP database and corrected for anthropogenic inputs).  
1057 Dotted lines are the calculated uncertainties based on errors on TA and DIC from the GLODAP database.

1058

1059 **Figure 5:** Boron isotopic measurements of mixed-layer foraminifera plotted against the  $\delta^{11}B_{borate}$ .  $\delta^{11}B_{borate}$  was  
1060 characterized by determination of the calcification depth of the foraminifera utilizing data presented in Fig. 4. A)  
1061 *G. ruber*, B) *T. sacculifer*, C) *O. universa*. Mono-specific calibrations (Table 3) and error bars on  $\delta^{11}B_{borate}$  were  
1062 derived utilizing the wild bootstrap code from Henehan et al. (2016), while errors on the  $\delta^{11}B_{carbonate}$  for this  
1063 study are reported as  $2\sigma$  of measured AE121 standards during the session of the sample. Calibrations were also  
1064 derived on the 250-400 size fraction for *G. ruber* and *T. sacculifer* (black dashed lines). Data reported on those  
1065 graphs have been measured with an MC-ICP-MS.

1066

1067 **Figure 6:** Boron isotopic measurements of deep-dwelling foraminifera ( $\delta^{11}B_{carbonate}$ ) plotted against  $\delta^{11}B_{borate}$ .  
1068  $\delta^{11}B_{borate}$  was constrained using foraminiferal calcification depths. A) *P. obliquiloculata*, B) *G. menardii*, C) *N.*  
1069 *dutertrei*, D) *G. tumida* and E) Compilation of deep dweller species. Mono-specific calibrations are summarized  
1070 in Table 3.

1071

1072 **Figure 7:** Boxplots of B/Ca ratios for multiple foraminifera species., including *T. sacculifer* (this study; Foster et  
1073 al., 2008; Ni et al.; 2007; Seki et al., 2010), *G. ruber* (this study; Babila et al., 2014; Foster et al., 2008; Ni et al.,  
1074 2007), *G. inflata*, *G. bulloides* (Yu et al., 2007), *N. pachyderma* (Hendry et al., 2009; Yu et al., 2013), *N.*  
1075 *dutertrei* (this study; Foster et al., 2008), *O. universa*, *P.obliquiloculata*, *G. menardii*, *G. tumida* (this study).

1076

1077 **Figure 8:** A) Boxplot showing the calculated microenvironment pH difference ( $\Delta$ microenvironment pH)  
1078 between microenvironment and external pH based on the  $\delta^{11}B$  data. B) This figure shows that a decrease in  
1079 insolation can explain the low  $\delta^{11}B$  from the WEP. Light penetration profile in the Western Pacific, with  $E_0$   
1080 in the WEP of  $220 J.s^{-1}.m^{-2}$  (Weare et al., 1981) and a light attenuation coefficient of  $0.028 (m^{-1})$  (Wang et al.,  
1081 2008). Theoretical depths were calculated for a decrease in microenvironment pH of  $\Delta pH_1 = -0.02$  (e.g. WP07-a);

1082  $\Delta\text{pH}_1 = -0.04$  (e.g. A14),  $\Delta\text{pH}_2 = -0.06$  (e.g. 806A). Light penetration corresponding to  $E_c$  is  $\sim 12\%$ ,  $\Delta\text{pH}_0 \sim 7\%$ ,  
1083  $\Delta\text{pH}_1 \sim 5\%$ ,  $\Delta\text{pH}_2 \sim 1\%$  respective calcification depth are 75m, 90m, 110m and 150m. Grey band is the  
1084 calcification depth calculated that explains the  $\Delta$  microenvironment pH from  $\Delta\text{pH}_0$  to  $\Delta\text{pH}_2$ . Dotted lines show  
1085 the range of the calcification depth for *T. sacculifer* (w/o sacc) in the WEP utilized in this study.

1086  
1087 **Figure 9:** Water depth pH profiles reconstructed at every site applying the mono-specific calibrations derived  
1088 from our results (Table 3). Figure is showing measured  $\delta^{11}\text{B}_{\text{calcite}}$ ,  $\delta^{11}\text{B}_{\text{borate}}$  calculated according to different  
1089 calibrations (see Table 3 and text), calculated pH based on  $\delta^{11}\text{B}$  ( $\text{pH}_{\delta^{11}\text{B}}$ ) and  $\text{pCO}_2$  calculated from  $\text{pH}_{\delta^{11}\text{B}}$  and  
1090 alkalinity.

1091  
1092 **Figure 10:** Evaluation of the reconstructed parameters,  $\delta^{11}\text{B}_{\text{borate}}$ , pH and  $\text{pCO}_2$  versus *in situ* parameter  
1093 calculated in Fig. 9 (based on  $\delta^{11}\text{B}$  and alkalinity). The recalculated parameters are consistent with *in situ* data,  
1094 except for *G. ruber*, and this variability might be explained by the different test sizes within measured size  
1095 fractions.

1096 **Table caption**

1097

1098 **Table 1:** Box-core information

1099

1100 **Table 2:** Analytical results of  $\delta^{13}\text{C}$ ,  $\delta^{18}\text{O}$ ,  $\delta^{11}\text{B}$  and elemental ratios Li/Ca, B/Ca and Mg/Ca

1101

1102 **Table 3:** Species-specific  $\delta^{11}\text{B}_{\text{carbonate}}$  to  $\delta^{11}\text{B}_{\text{borate}}$  calibrations from literature and from our data

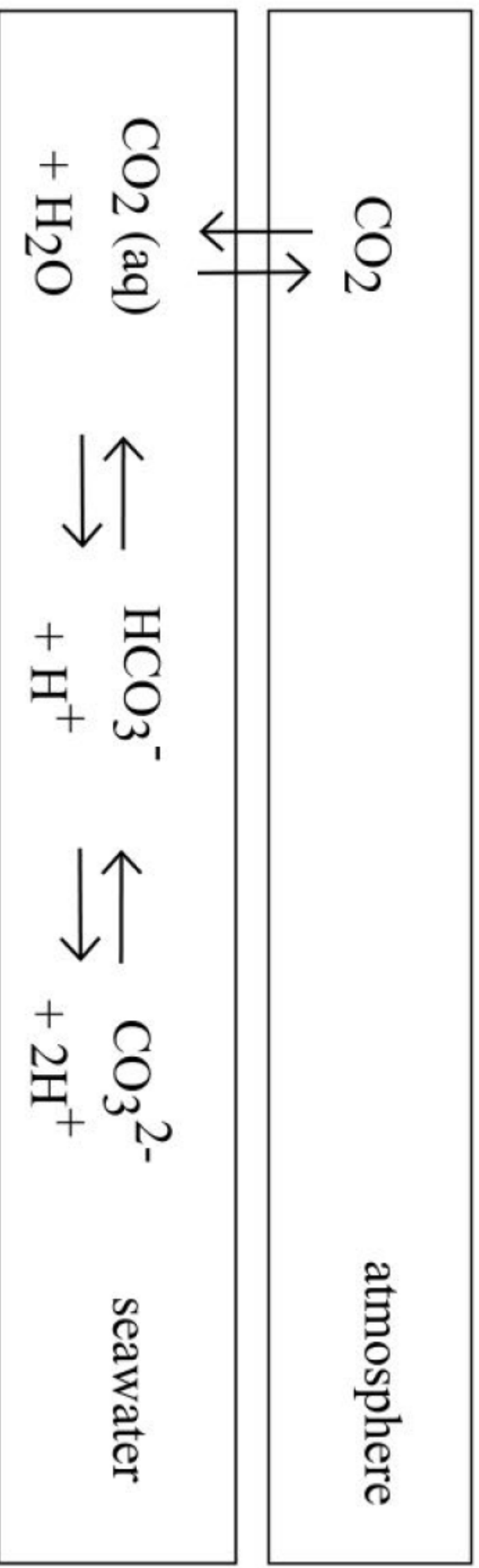


**Figure 1**



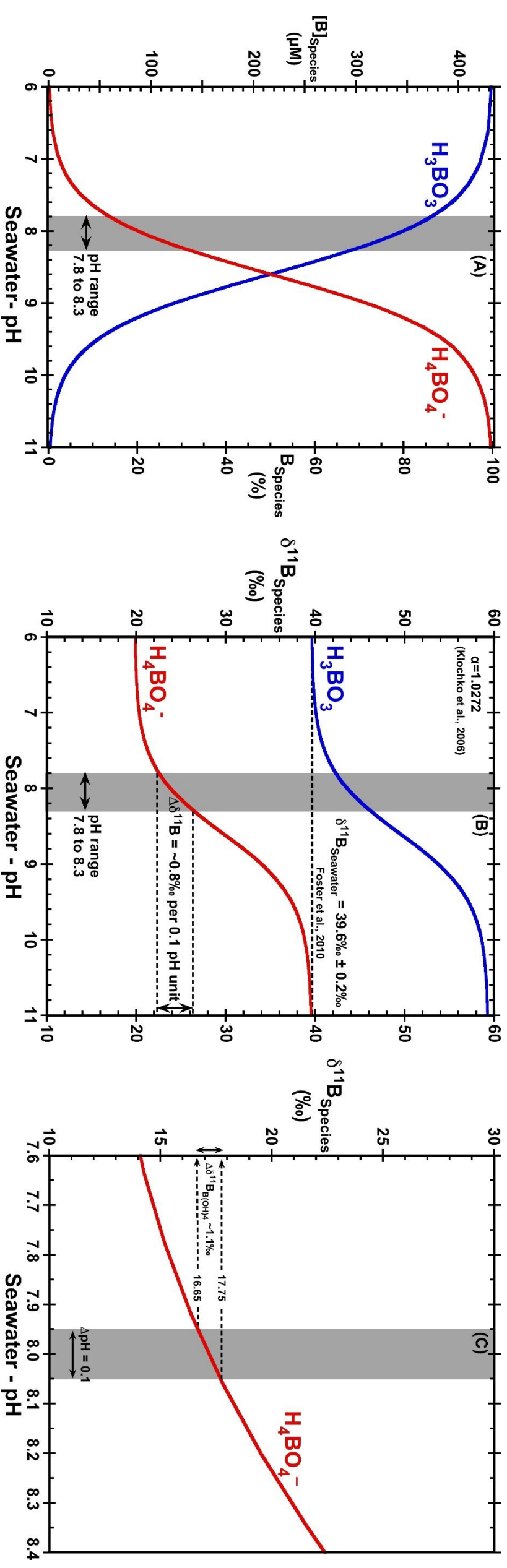


Figure 2

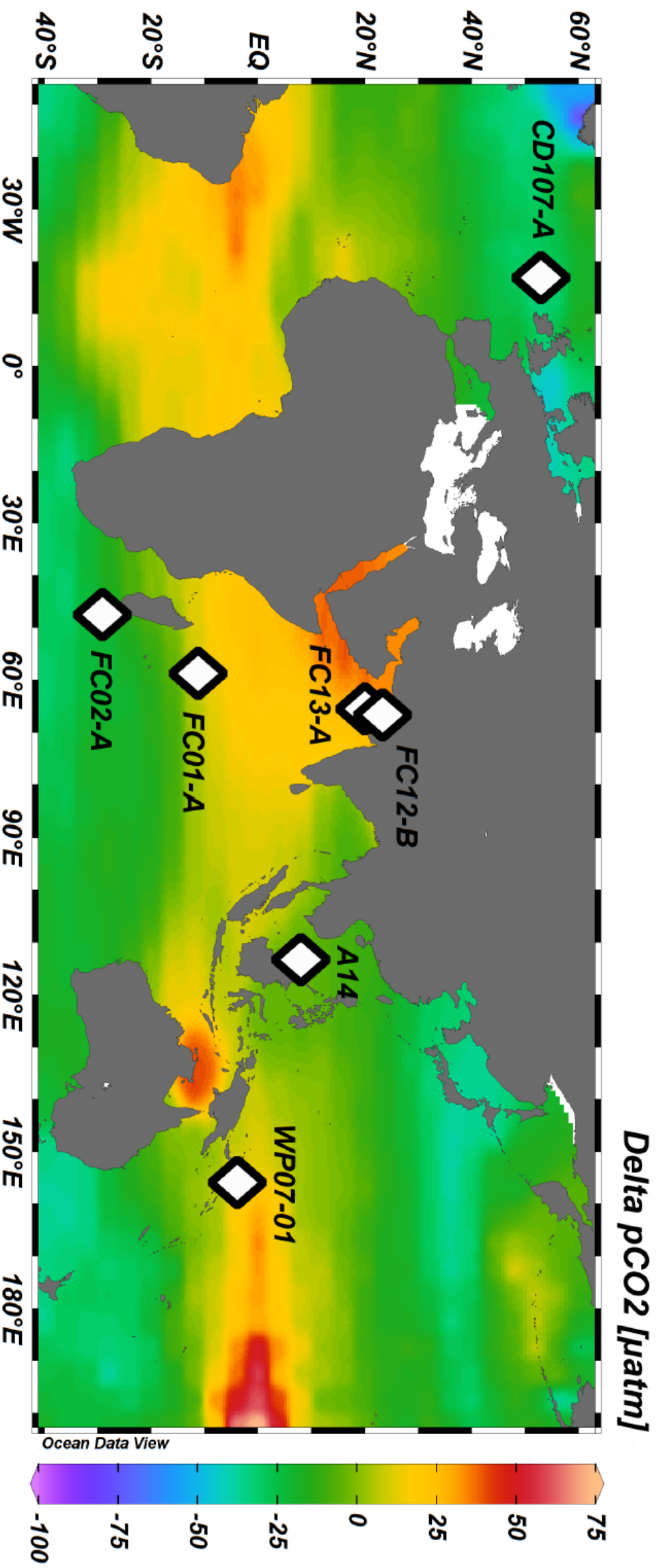


Figure 3

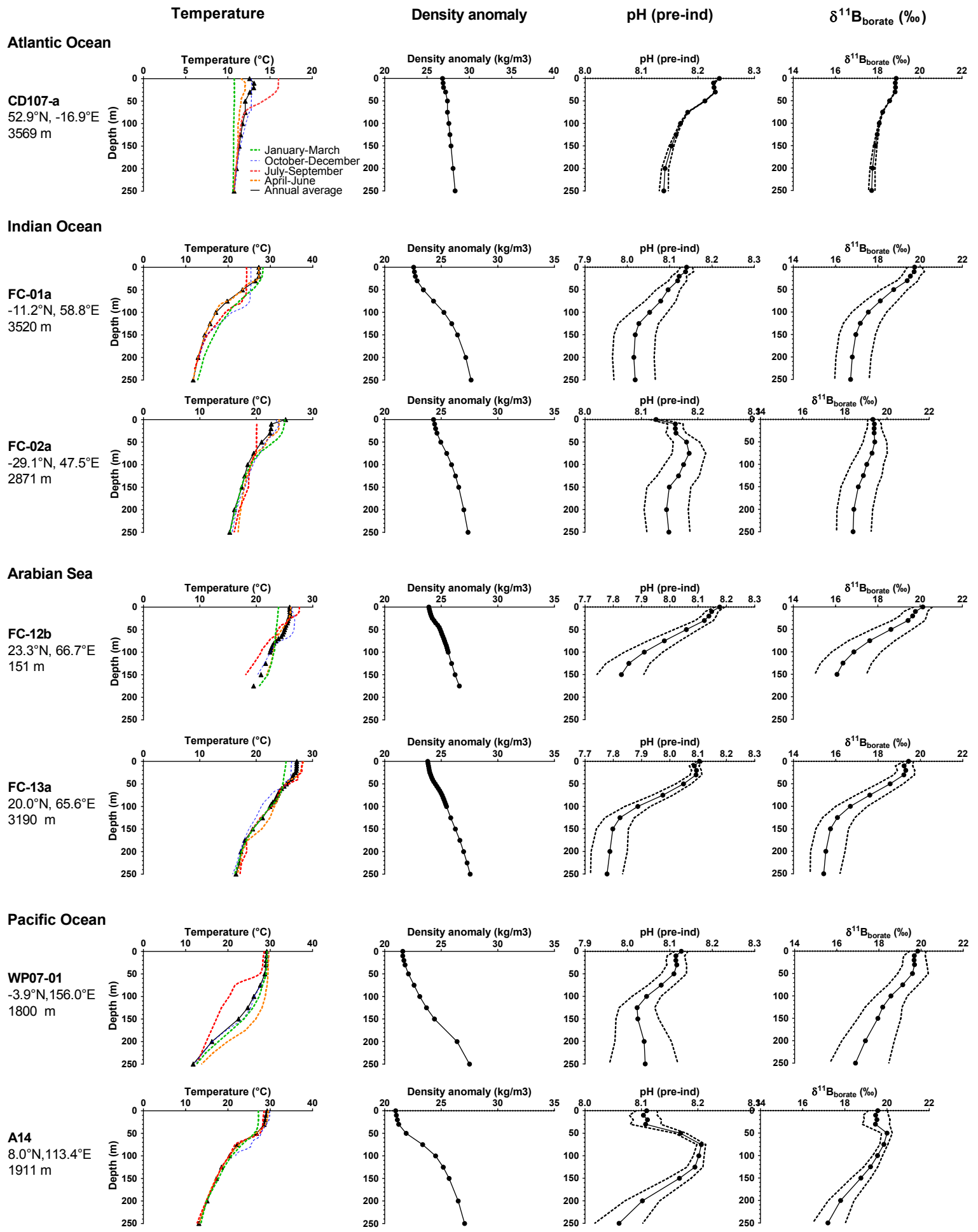
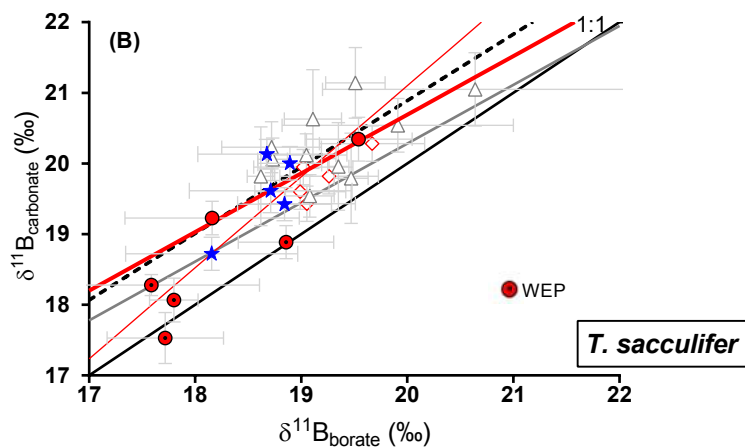
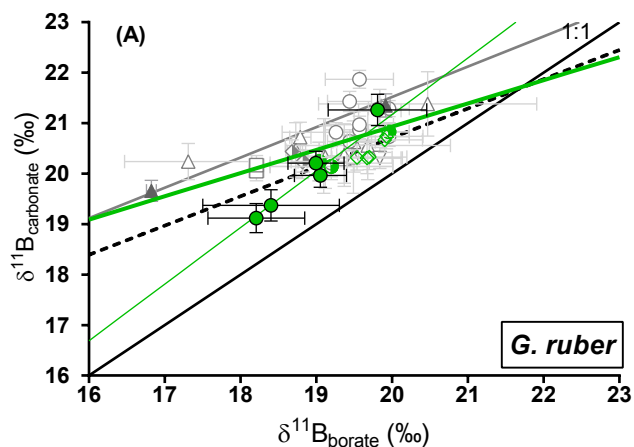
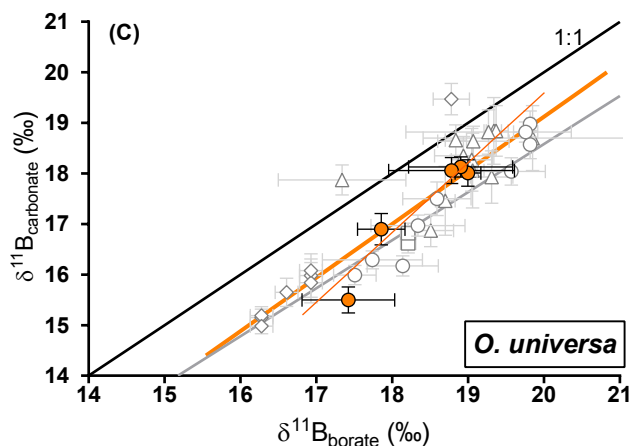


Figure 4 35



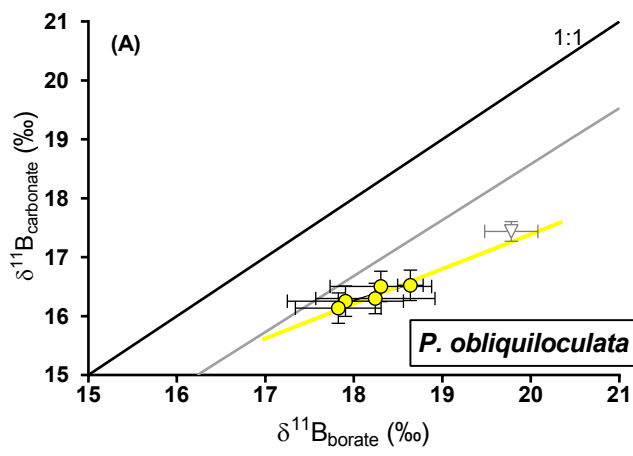
- $\delta^{11}\text{B}_{G. ruber}$  (core-top, 250-400 $\mu\text{m}$ , this study)
- ◇  $\delta^{11}\text{B}_{G. ruber}$  (core-top, 300-355 $\mu\text{m}$ , Foster et al., 2008)
- $\delta^{11}\text{B}_{G. ruber}$  (core-top, 250-300 $\mu\text{m}$ , Henehan et al., 2013)
- $\delta^{11}\text{B}_{G. ruber}$  (core-top, 250-455 $\mu\text{m}$ , Henehan et al., 2013)
- $\delta^{11}\text{B}_{G. ruber}$  (sediment trap, 250-355 $\mu\text{m}$ , Henehan et al., 2013)
- ◇  $\delta^{11}\text{B}_{G. ruber}$  (tow, Henehan et al., 2013)
- ▲  $\delta^{11}\text{B}_{G. ruber}$  (culture, Henehan et al., 2013)
- ▽  $\delta^{11}\text{B}_{G. ruber}$  (grab sample, 250-355 $\mu\text{m}$ , Henehan et al., 2013)
- △  $\delta^{11}\text{B}_{G. ruber}$  (core-top, 315-355 $\mu\text{m}$ , Raizsch et al., 2018)
- $G. ruber$  calibration line (all data, this study, 250-455)
- $G. ruber$  calibration line (core-top, this study, 250-400 $\mu\text{m}$ )
- $G. ruber$  calibration line (culture, Henehan et al., 2013)
- - -  $G. ruber$  calibration line (this study, 250-300 $\mu\text{m}$  from Henehan et al., 2013)

- $\delta^{11}\text{B}_{T. sacculifer}$  (w/o sacc) (core-top, 250-400 $\mu\text{m}$ , this study)
- △  $\delta^{11}\text{B}_{T. sacculifer}$  (w/o sacc) (core-top, 315-355 $\mu\text{m}$ , Raizsch et al., 2018)
- ★  $\delta^{11}\text{B}_{T. sacculifer}$  (sacc) (core-top, 250-400 $\mu\text{m}$ , this study)
- ◇  $\delta^{11}\text{B}_{T. sacculifer}$  (sacc) (core-top, 500-600 $\mu\text{m}$ , Foster et al., 2008)
- $T. sacculifer$  (w/o sacc and sacc) calibration line (all data, 250-600 $\mu\text{m}$ , this study)
- $T. sacculifer$  (w/o sacc and sacc) calibration line (core-top, 250-400 $\mu\text{m}$ , this study)
- $T. sacculifer$  (sacc) calibration line (Martinez-Boti et al., 2015)
- - -  $T. sacculifer$  (w/o sacc and sacc) calibration line 250-400  $\mu\text{m}$  (this study and Raizsch et al., 2018)

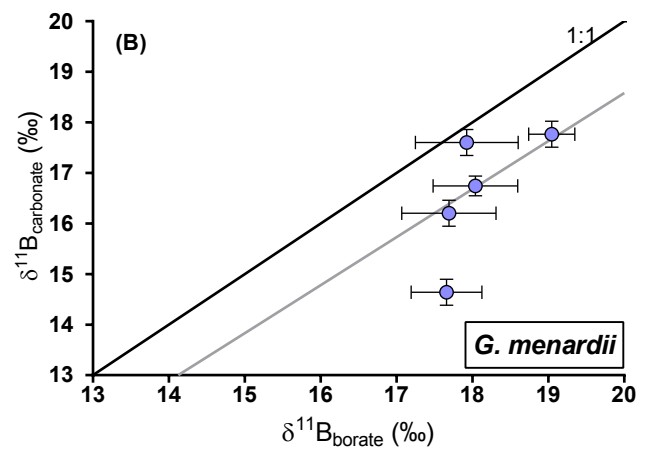


- $\delta^{11}\text{B}_{O. universa}$  (core-top, this study)
- $\delta^{11}\text{B}_{O. universa}$  (core-top, Henehan et al., 2016)
- $\delta^{11}\text{B}_{O. universa}$  (sediment trap, Henehan et al., 2016)
- ◇  $\delta^{11}\text{B}_{O. universa}$  (tow, Henehan et al., 2016)
- △  $\delta^{11}\text{B}_{O. universa}$  (core-top, Raizsch et al., 2018)
- $O. universa$  calibration line (core-top, this study)
- $O. universa$  calibration line (this study, Henehan et al., 2016, Raizsch et al., 2018)
- $O. universa$  calibration line (wild, Henehan et al., 2016)

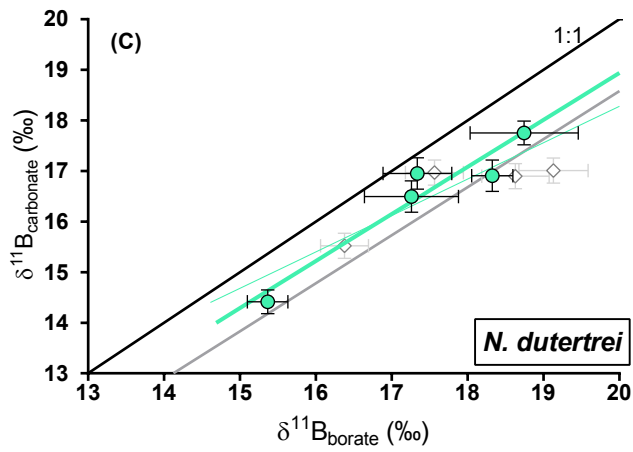
Figure 5



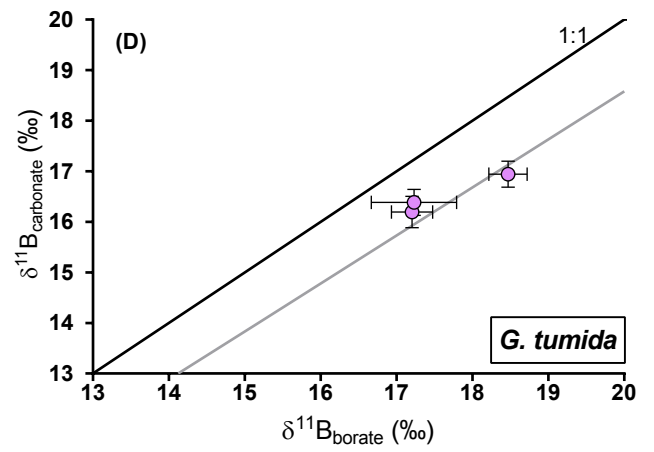
- $\delta^{11}\text{B}_{P.obliquiloculata}$  (Core-top, this study)
- ▽  $\delta^{11}\text{B}_{P.obliquiloculata}$  (Henehan et al., 2016)
- $P.obliquiloculata$  calibration line (this study, Henehan et al., 2016)
- $O.universa$  calibration curve (Henehan et al., 2016)



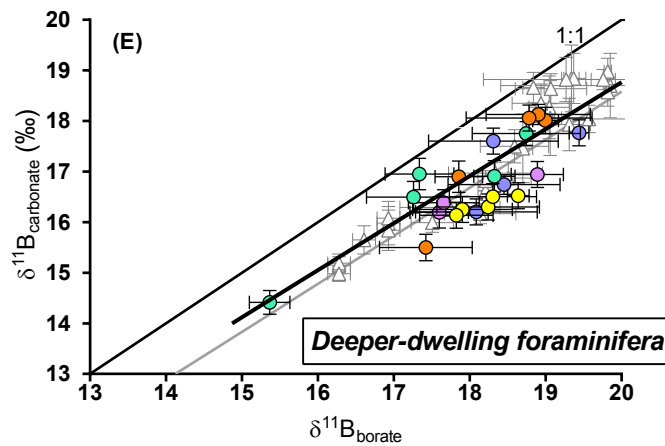
- $\delta^{11}\text{B}_{G.menardii}$  (this study)
- $O.universa$  calibration curve (Henehan et al., 2016)



- $\delta^{11}\text{B}_{N.dutertrei}$  (Core-top, this study)
- ◇  $\delta^{11}\text{B}_{N.dutertrei}$  (Core-top, Foster et al., 2008)
- $O.universa$  calibration line (This study)
- $O.universa$  calibration line (This study, Foster et al., 2008)
- $O.universa$  calibration line (Henehan et al., 2016)



- $\delta^{11}\text{B}_{G.tumida}$  (this study)
- $O.universa$  calibration curve (Henehan et al., 2016)



- $\delta^{11}\text{B}_{O.universa}$
- $\delta^{11}\text{B}_{P.obliquiloculata}$
- $\delta^{11}\text{B}_{N.dutertrei}$
- $\delta^{11}\text{B}_{G.menardii}$
- $\delta^{11}\text{B}_{G.tumida}$
- △  $\delta^{11}\text{B}_{\text{deep-dweller}}$  from literature
- Deep-dweller calibration line
- $O.universa$  calibration line (Henehan et al., 2016)

Figure 6 37

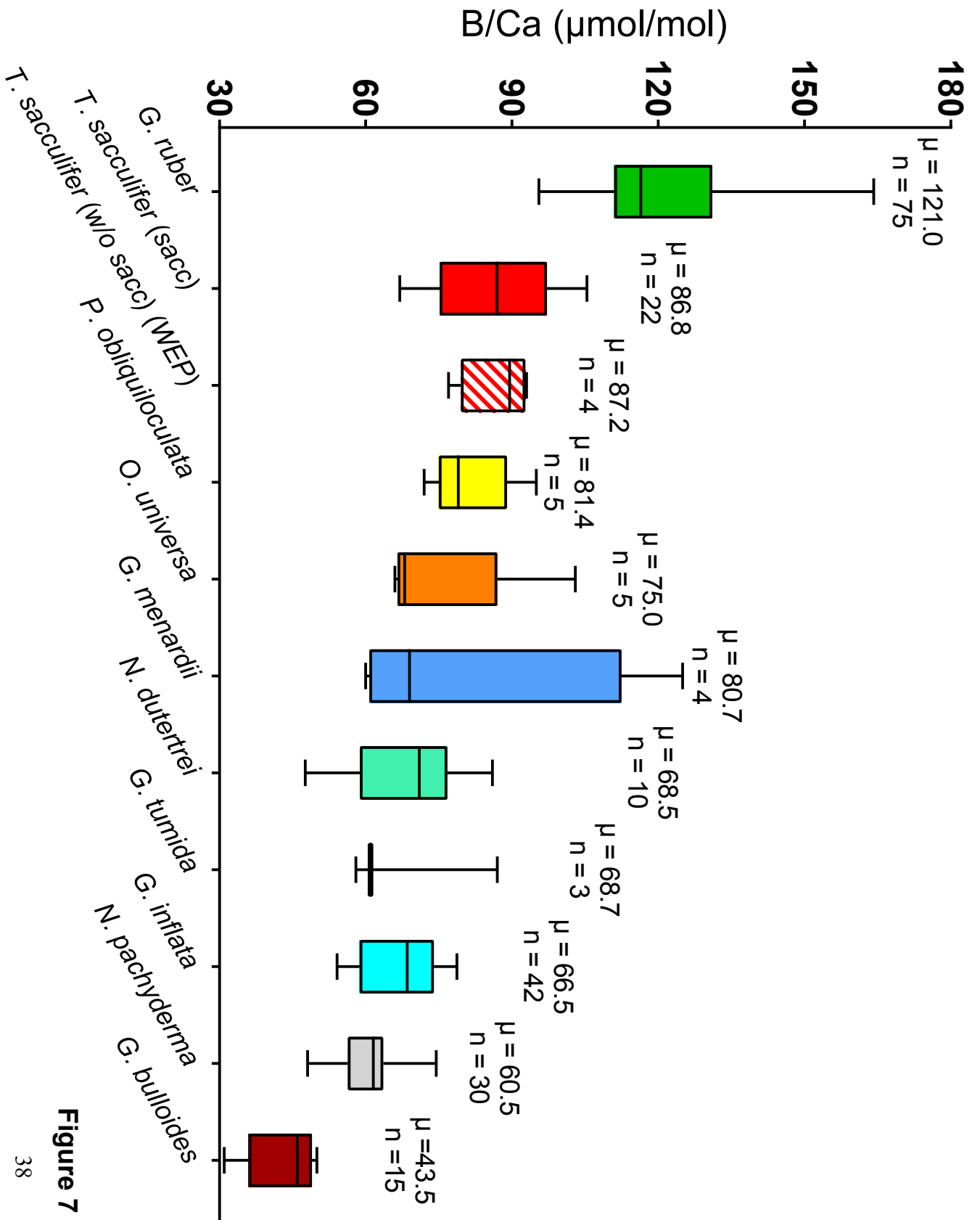


**Figure 7**

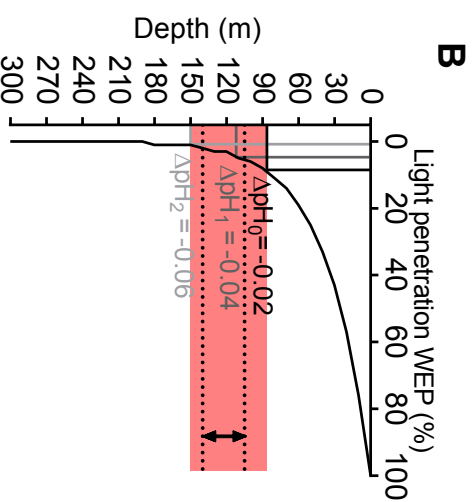
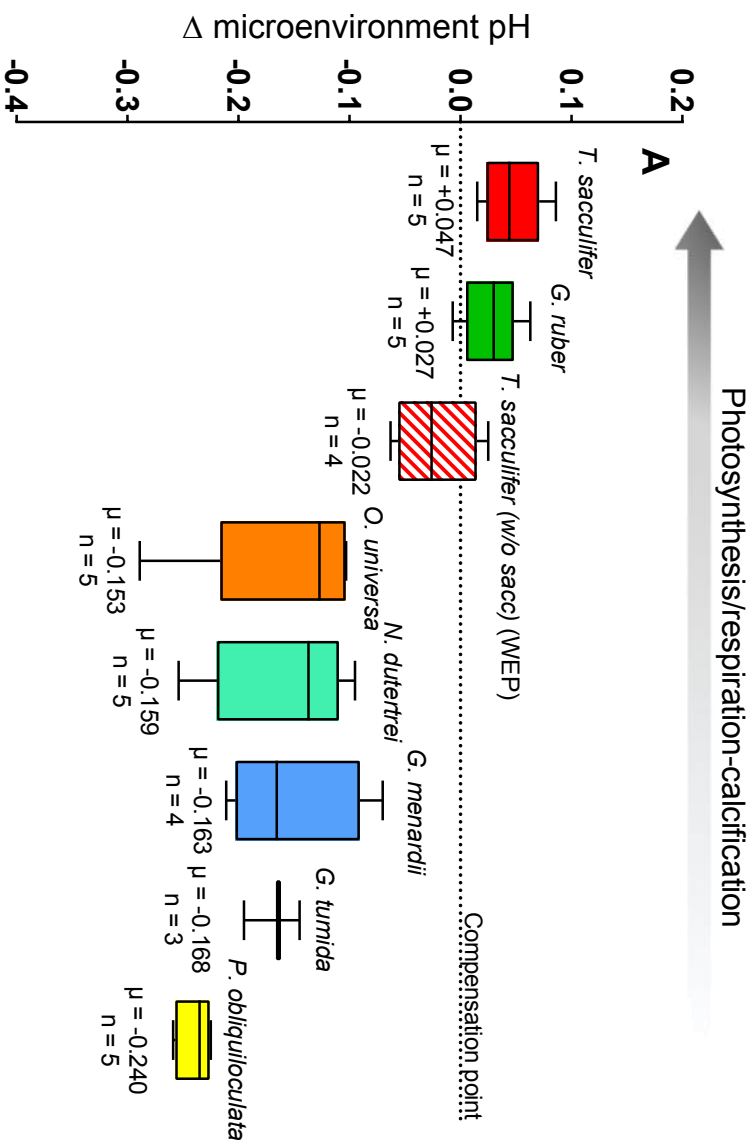


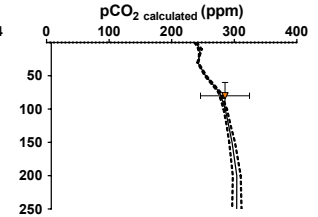
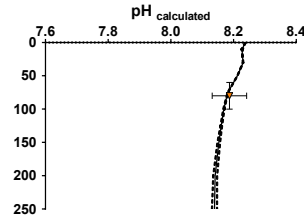
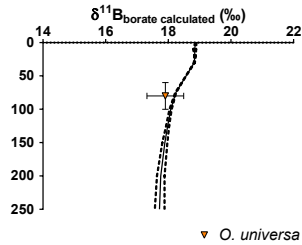
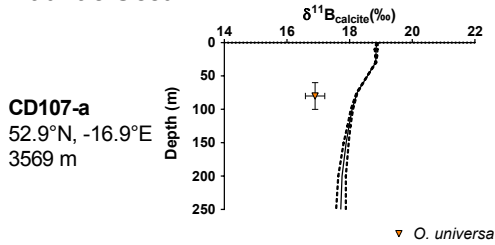
**Figure 8**

$\delta^{11}\text{B}_{\text{carbonate}}$  $\delta^{11}\text{B}_{\text{borate}}$ 

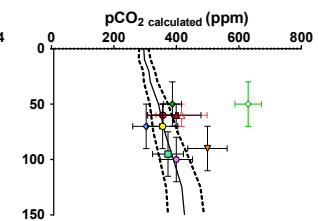
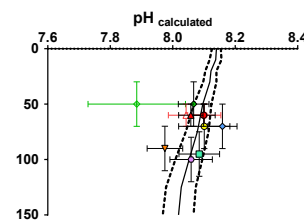
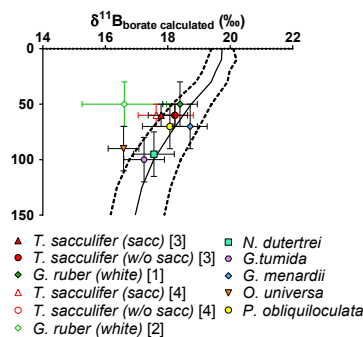
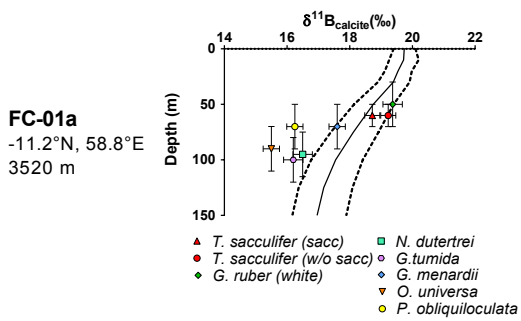
pH

 $\text{pCO}_2$ 

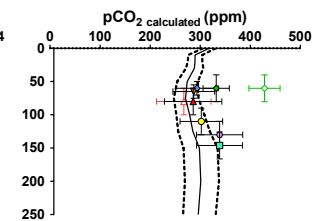
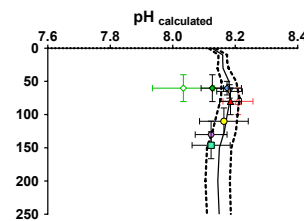
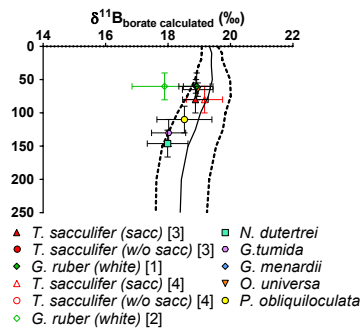
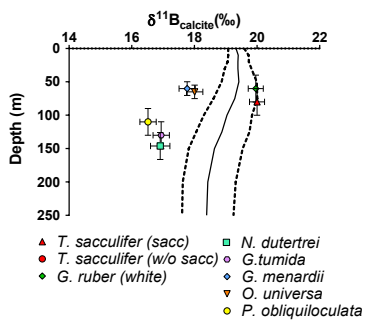
## Atlantic Ocean



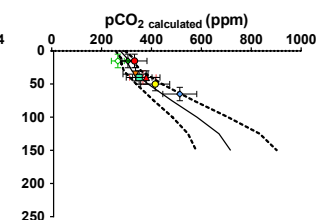
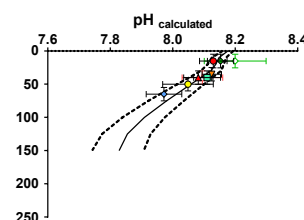
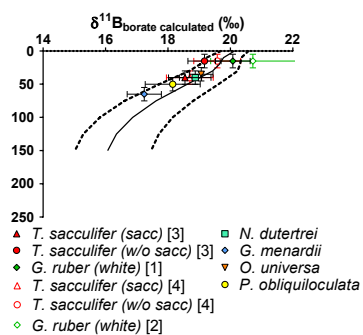
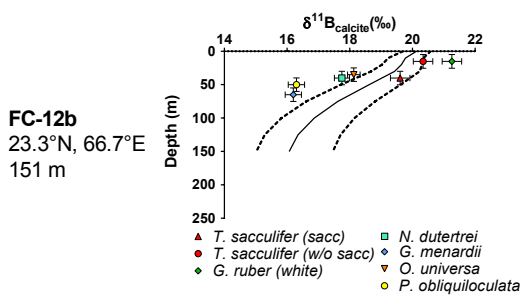
## Indian Ocean



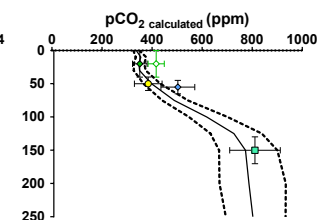
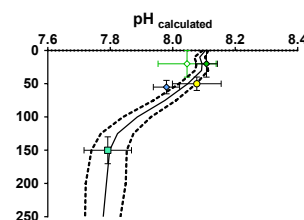
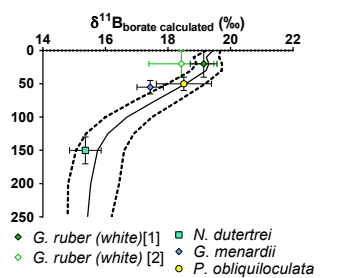
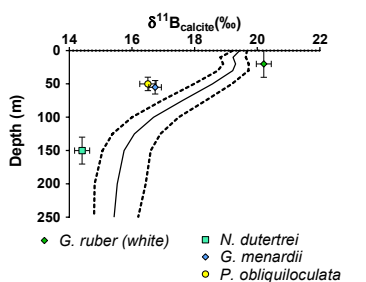
**FC-02a**  
-29.1°N, 47.5°E  
2871 m



## Arabian Sea



**FC-13a**  
20.0°N, 65.6°E  
3190 m



## Pacific Ocean

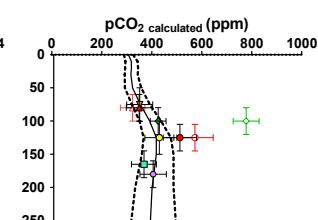
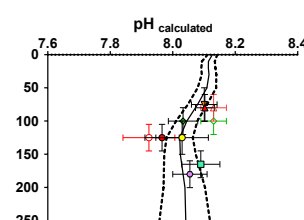
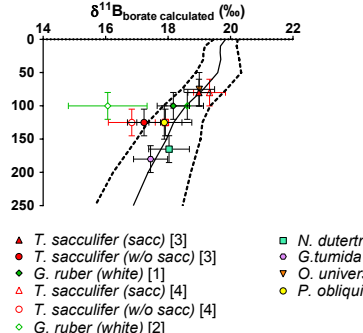
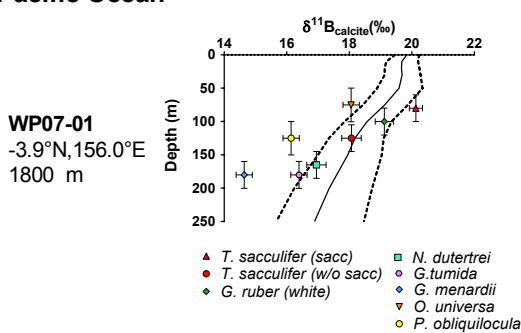
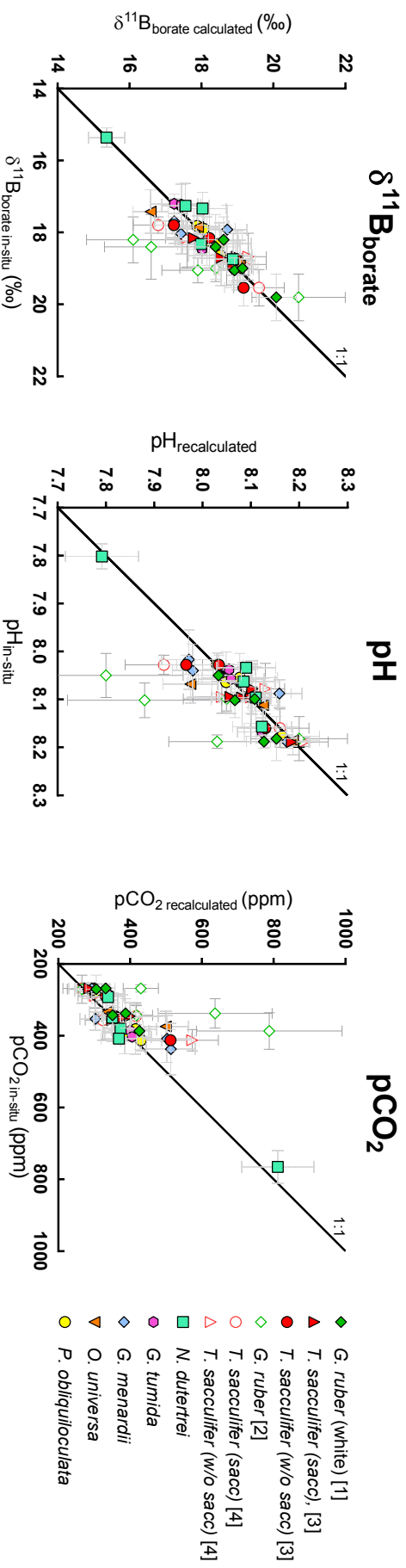


Figure 9





**Figure 10**

**Table 1**

<b>Label</b>	<b>Box-Core</b>	<b>Site</b>	<b>Latitude (N)</b>	<b>Longitude (E)</b>	<b>Depth (mbsl)</b>	<b>Oceanic Regime</b>	<b><math>\Delta^{14}\text{C}</math> age (year)</b>
<i>Atlantic Ocean</i>							
CD107-a	CD107	A	52.92	-16.92	3569	non-upwelling	<3000 <sup>a</sup>
<i>Indian Ocean</i>							
FC-01a	WIND-33B	I	-11.21	58.77	3520	non-upwelling	
FC-02a	WIND-10B	K	-29.12	47.55	2871	non-upwelling	7252 ± 27 <sup>b</sup>
<i>Arabian Sea</i>							
FC-12b	CD145	A150	23.30	66.70	151	seasonal upwelling	
FC-13a	CD145	A3200	20.00	65.58	3190	seasonal upwelling	
<i>Pacific Ocean</i>							
WP07-01			-3.93	156.00	1800	non-upwelling	7.3-8.6 <sup>c</sup>
A14			8.02	113.39	1911	non-upwelling	7.3-8.6 <sup>c</sup>
806		A	0.32	159.36	2521	equatorial divergence	7.3-8.6 <sup>c</sup>
807		A	3.61	156.62	2804	equatorial divergence	7.3-8.6 <sup>c</sup>

<sup>a</sup>Thomson et al., 2000

<sup>b</sup>Wilson et al., 2012

<sup>c</sup>Age for core-top of site 806B from Lea et al., 2000

Table 2

Core	Species	Fraction size (µm)	$\delta^{13}\text{C}^s$ (‰)	$\delta^{18}\text{O}^s$ (‰)	$\delta^{11}\text{Bc}$ (‰)	$\delta^{11}\text{Bc}$ (‰)	$\delta^{11}\text{B}_{\text{average}}^{**}$ (‰)	$\text{Li/Ca}^{***}$ (µmol/mol)	$\text{B/Ca}^{***}$ (µmol/mol)	$\text{Mg/Ca}^{***}$ (µmol/mol)	
<b>Atlantic Ocean</b>											
CD107a	<i>O. universa</i>	>500	1.99 ± 0.03	1.25 ± 0.11	16.85 ± 0.31 (2SD, n=AE12=11)	16.95 ± 0.31 (2SD, n=AE12=11)	16.90 ± 0.22	13.9 ± 0.4	68 ± 7	3.60 ± 0.01	
<b>Indian Ocean</b>											
FC-01a	<i>G. ruber</i> (white ss)	250-300	1.37 ± 0.03	-1.32 ± 0.11	19.33 ± 0.31 (2SD, n=AE12=11)	19.41 ± 0.31 (2SD, n=AE12=11)	19.37 ± 0.22	15.4 ± 0.4	109 ± 7	3.98 ± 0.01	
FC-01a	<i>T. sacculifer</i> (sacc)	300-400	1.88 ± 0.03	-2.20 ± 0.11	18.71 ± 0.24 (2SD, n=AE12=10)	18.73 ± 0.24 (2SD, n=AE12=10)	18.72 ± 0.17	12.1 ± 0.4	87 ± 7	3.45 ± 0.01	
FC-01a	<i>T. sacculifer</i> (w/o sacc)	300-400	2.02 ± 0.03	-1.05 ± 0.11	19.13 ± 0.24 (2SD, n=AE12=10)	19.32 ± 0.24 (2SD, n=AE12=10)	19.23 ± 0.17	12.1 ± 0.4	82 ± 7	3.42 ± 0.01	
FC-01a	<i>O. universa</i>	>500			15.50 ± 0.26 (2SD, n=AE12=14)		15.50 ± 0.26				
FC-01a	<i>P. obliquiloculata</i>	300-400	1.00 ± 0.03	-0.55 ± 0.11	16.40 ± 0.26 (2SD, n=AE12=14)	16.10 ± 0.26 (2SD, n=AE12=14)	16.25 ± 0.18	15.4 ± 0.4	78 ± 7	2.06 ± 0.01	
FC-01a	<i>G. menardi</i>	300-400	1.64 ± 0.03	0.43 ± 0.11	17.52 ± 0.26 (2SD, n=AE12=14)	17.69 ± 0.26 (2SD, n=AE12=14)	17.60 ± 0.18	12.7 ± 0.4	63 ± 7	2.26 ± 0.01	
FC-01a	<i>N. duterrei</i>	300-400	1.28 ± 0.03	-0.43 ± 0.11	16.40 ± 0.31 (2SD, n=AE12=11)	16.59 ± 0.31 (2SD, n=AE12=11)	16.50 ± 0.22	18.6 ± 0.4	73 ± 7	1.81 ± 0.01	
FC-01a	<i>G. tumida</i>	300-400	1.29 ± 0.03	-0.53 ± 0.11	16.21 ± 0.31 (2SD, n=AE12=11)	16.18 ± 0.31 (2SD, n=AE12=11)	16.20 ± 0.22	10.0 ± 0.4	61 ± 7	1.79 ± 0.01	
FC-02a	<i>G. ruber</i> (white ss)	250-300	0.30 ± 0.03	-1.40 ± 0.11	20.02 ± 0.24 (2SD, n=AE12=10)	19.90 ± 0.24 (2SD, n=AE12=10)	19.96 ± 0.17	18.2 ± 0.4	125 ± 7	3.47 ± 0.01	
FC-02a	<i>T. sacculifer</i> (sacc)	300-400	1.43 ± 0.03	-1.60 ± 0.11	20.07 ± 0.24 (2SD, n=AE12=10)	19.93 ± 0.24 (2SD, n=AE12=10)	20.00 ± 0.17	14.2 ± 0.4	106 ± 7	3.30 ± 0.01	
FC-02a	<i>T. sacculifer</i> (w/o sacc)	300-400	1.52 ± 0.03	-1.40 ± 0.11	23.23 ± 0.24 (2SD, n=AE12=10)	23.22 ± 0.24 (2SD, n=AE12=10)	23.22 ± 0.17	13.7 ± 0.4	106 ± 7	3.34 ± 0.01	
FC-02a	<i>O. universa</i>	>500	1.79 ± 0.03	0.02 ± 0.11	18.05 ± 0.26 (2SD, n=AE12=14)	17.97 ± 0.26 (2SD, n=AE12=14)	18.01 ± 0.18	14.8 ± 0.4	67 ± 7	4.40 ± 0.01	
FC-02a	<i>P. obliquiloculata</i>	300-400	0.34 ± 0.03	0.56 ± 0.11	16.35 ± 0.26 (2SD, n=AE12=14)	16.69 ± 0.26 (2SD, n=AE12=14)	16.52 ± 0.18	16.6 ± 0.4	83 ± 7	2.33 ± 0.01	
FC-02a	<i>G. menardi</i>	300-400	1.73 ± 0.03	-0.51 ± 0.11	17.77 ± 0.26 (2SD, n=AE12=14)	17.77 ± 0.26 (2SD, n=AE12=14)	17.77 ± 0.26	15.8 ± 0.4	125 ± 7	2.21 ± 0.01	
FC-02a	<i>N. duterrei</i>	300-400	1.03 ± 0.03	-0.55 ± 0.11	16.78 ± 0.31 (2SD, n=AE12=11)	17.03 ± 0.31 (2SD, n=AE12=11)	16.91 ± 0.22	18.6 ± 0.4	82 ± 7	2.13 ± 0.01	
FC-02a	<i>G. tumida</i>	300-400	1.64 ± 0.03	-0.28 ± 0.11	16.93 ± 0.26 (2SD, n=AE12=14)	16.95 ± 0.26 (2SD, n=AE12=14)	16.94 ± 0.18	15.6 ± 0.4	87 ± 7	1.90 ± 0.01	
<b>Arabian Sea</b>											
FC-12b	<i>G. ruber</i> (white ss)	250-300	0.58 ± 0.03	-2.82 ± 0.11	21.30 ± 0.31 (2SD, n=AE12=11)	21.23 ± 0.31 (2SD, n=AE12=11)	21.26 ± 0.22	19.5 ± 0.4	164 ± 7	5.76 ± 0.01	
FC-12b	<i>G. sacculifer</i> (s)	300-400	1.76 ± 0.03	-2.15 ± 0.11	19.65 ± 0.31 (2SD, n=AE12=11)	19.57 ± 0.31 (2SD, n=AE12=11)	19.61 ± 0.22	14.6 ± 0.4	101 ± 7	4.28 ± 0.01	
FC-12b	<i>T. sacculifer</i> (w/o sacc)	300-400	1.97 ± 0.03	-2.19 ± 0.11	20.32 ± 0.31 (2SD, n=AE12=11)	20.37 ± 0.31 (2SD, n=AE12=11)	20.34 ± 0.22	16.7 ± 0.4	116 ± 7	4.90 ± 0.01	
FC-12b	<i>O. universa</i>	>500	1.89 ± 0.03	-1.59 ± 0.11	18.13 ± 0.20 (2SD, n=AE12=6)	18.13 ± 0.20 (2SD, n=AE12=6)	18.13 ± 0.20	13.6 ± 0.4	103 ± 7	6.91 ± 0.01	
FC-12b	<i>P. obliquiloculata</i>	300-400	0.5 ± 0.03	-1.58 ± 0.11	16.45 ± 0.26 (2SD, n=AE12=14)	16.15 ± 0.26 (2SD, n=AE12=14)	16.30 ± 0.18	16.7 ± 0.4	95 ± 7	3.61 ± 0.01	
FC-12b	<i>G. menardi</i>	300-400	1.05 ± 0.03	-0.97 ± 0.11	16.2 ± 0.26 (2SD, n=AE12=14)	16.2 ± 0.26 (2SD, n=AE12=14)	16.20 ± 0.26	14.8 ± 0.4	75 ± 7	3.44 ± 0.01	
FC-12b	<i>N. duterrei</i>	300-400	1.35 ± 0.03	-1.57 ± 0.11	17.77 ± 0.24 (2SD, n=AE12=10)	17.73 ± 0.24 (2SD, n=AE12=10)	17.75 ± 0.17	17.1 ± 0.4	75 ± 7	3.25 ± 0.01	
FC-13a	<i>G. ruber</i> (white ss)	250-300	0.08 ± 0.03	-3.71 ± 0.11	20.27 ± 0.24 (2SD, n=AE12=10)	20.15 ± 0.24 (2SD, n=AE12=10)	20.21 ± 0.17	16.4 ± 0.4	147 ± 7	4.52 ± 0.01	
FC-13a	<i>T. sacculifer</i> (w/o sacc)	300-400	1.59 ± 0.03	-2.46 ± 0.11	17.85 ± 0.29 (2SD, n=AE12=12)	17.85 ± 0.29 (2SD, n=AE12=12)	17.85 ± 0.29	15.7 ± 0.4	121 ± 7	5.49 ± 0.01	
FC-13a	<i>P. obliquiloculata</i>	300-400	0.00 ± 0.03	-0.97 ± 0.11	16.51 ± 0.26 (2SD, n=AE12=14)	16.50 ± 0.26 (2SD, n=AE12=14)	16.51 ± 0.18	18.7 ± 0.4	79 ± 7	4.43 ± 0.01	
FC-13a	<i>G. menardi</i>	300-400	0.75 ± 0.03	-1.07 ± 0.11	16.74 ± 0.20 (2SD, n=AE12=6)	16.74 ± 0.20 (2SD, n=AE12=6)	16.74 ± 0.20	9.2 ± 0.4	60 ± 7	1.99 ± 0.01	
FC-13a	<i>N. duterrei</i>	300-400	0.71 ± 0.03	-1.41 ± 0.11	14.43 ± 0.24 (2SD, n=AE12=10)	14.40 ± 0.24 (2SD, n=AE12=10)	14.41 ± 0.17	15.7 ± 0.4	69 ± 7	1.98 ± 0.01	
<b>Pacific Ocean</b>											
WP07-a	<i>G. ruber</i> (white ss)	250-400			19.12 ± 0.29 (2SD, n=AE12=12)		19.12 ± 0.29	14.5 ± 0.4	144 ± 7	4.32 ± 0.01	
WP07-a	<i>T. sacculifer</i> (sacc)	250-400			20.13 ± 0.21 (2SD, n=AE12=11)		20.13 ± 0.21	12.7 ± 0.4	92 ± 7	4.44 ± 0.01	
WP07-a	<i>T. sacculifer</i> (w/o sacc)	250-400			18.10 ± 0.31 (2SD, n=AE12=11)		18.07 ± 0.22	12.3 ± 0.4	192 ± 7	4.51 ± 0.01	
WP07-a	<i>O. universa</i>	500-630			18.13 ± 0.26 (2SD, n=AE12=14)		17.99 ± 0.26 (2SD, n=AE12=14)	11.9 ± 0.4	71 ± 7	7.52 ± 0.01	
WP07-a	<i>P. obliquiloculata</i>	250-400			16.08 ± 0.26 (2SD, n=AE12=14)		16.19 ± 0.26 (2SD, n=AE12=14)	13.4 ± 0.4	72 ± 7	3.02 ± 0.01	
WP07-a	<i>G. menardi</i>	250-400			14.74 ± 0.26 (2SD, n=AE12=14)		14.53 ± 0.26 (2SD, n=AE12=14)	13.5 ± 0.4	85 ± 7	2.68 ± 0.01	
WP07-a	<i>N. duterrei</i>	250-400			16.91 ± 0.31 (2SD, n=AE12=11)		16.99 ± 0.31 (2SD, n=AE12=11)	21.7 ± 0.4	86 ± 7	3.66 ± 0.01	
WP07-a	<i>G. tumida</i>	250-400			16.45 ± 0.26 (2SD, n=AE12=14)		16.32 ± 0.26 (2SD, n=AE12=14)	10.6 ± 0.4	58 ± 7	2.55 ± 0.01	
806A	<i>T. sacculifer</i> (w/o sacc)	250-400			17.53 ± 0.36 (2SD, n=AE12=11)		17.53 ± 0.36	14.40 ± 0.4	77 ± 7	3.89 ± 0.01	
807A	<i>T. sacculifer</i> (w/o sacc)	250-400			18.38 ± 0.21 (2SD, n=AE12=11)		18.17 ± 0.21 (2SD, n=AE12=11)	12.54 ± 0.4	87 ± 7	4.24 ± 0.01	
A14	<i>G. ruber</i> (white ss)	250-400			18.91 ± 0.24 (2SD, n=AE12=10)		19.17 ± 0.24 (2SD, n=AE12=10)	19.04 ± 0.17	102 ± 7	3.91 ± 0.01	
A14	<i>T. sacculifer</i> (sacc)	250-400			19.53 ± 0.24 (2SD, n=AE12=10)		19.32 ± 0.24 (2SD, n=AE12=10)	19.42 ± 0.17	93 ± 7	3.76 ± 0.01	
A14	<i>T. sacculifer</i> (w/o sacc)	250-400			18.93 ± 0.24 (2SD, n=AE12=10)		18.84 ± 0.24 (2SD, n=AE12=10)	18.88 ± 0.17	12.3 ± 0.4	66 ± 7	6.59 ± 0.01
A14	<i>O. universa</i>	500-560			17.33 ± 0.26 (2SD, n=AE12=14)		17.08 ± 0.26 (2SD, n=AE12=14)	17.20 ± 0.18	11.3 ± 0.4	75 ± 7	1.99 ± 0.01
A14	<i>N. duterrei</i>	250-400			14.39 ± 0.31 (2SD, n=AE12=11)		14.39 ± 0.31	16.9 ± 0.4	75 ± 7	1.99 ± 0.01	

\* uncertainties given in 1SD (see text)

\*\* When two measurements were carried out uncertainty was calculated with  $\Delta a = \sqrt{(\sum (1/\Delta a_i)^2)}$ , with only one measurement the error was determined on reproducibility of the AE121 standard

\*\*\*Uncertainty given in 2SD, calculated on the reproducibility of CamWuellerstoff (see text and table S3, ref in Misra et al., 2014)

Table 3

Species	Size Fraction ( $\mu\text{m}$ )	Material	Instrument (original)	Regression method	$\delta^{11}\text{B}_{\text{meas}} (\delta^{11}\text{B}_{\text{lake}})$	n	Calibration number	Reference
<i>G. ruber</i>	~380	Culture/core tops/plankton tows	MC-ICP-MS	Bootstrap	$\delta^{11}\text{B}_{\text{meas}} = \delta^{11}\text{B}_{\text{lake}} - 9.52 (\pm 2.02) / 0.6 (\pm 0.11)$	9	0	This study; Henahan et al., 2013
<i>G. ruber</i>	315-355	Core-tops	MC-ICP-MS	Bootstrap	$\delta^{11}\text{B}_{\text{meas}} = \delta^{11}\text{B}_{\text{lake}} - 11.78 (\pm 3.20) / 0.45 (\pm 0.16)$	5	1	Rätzsch et al., 2018
<i>T. sacculifer</i>	n.d.	Culture/artificial seawater enriched in B	N-TIMS	Bootstrap	$\delta^{11}\text{B}_{\text{meas}} = \delta^{11}\text{B}_{\text{lake}} - 3.94 (\pm 4.02) / 0.82 (\pm 0.22)$	40	2	Sanyal et al., 2001; refitted; Martinez-Boit et al., 2015
<i>T. sacculifer</i>	315-355	Core-tops	MC-ICP-MS	Bootstrap	$\delta^{11}\text{B}_{\text{meas}} = \delta^{11}\text{B}_{\text{lake}} - 8.86 (\pm 5.27) / 0.59 (\pm 0.21)$	11	3	Rätzsch et al., 2018
<i>O. universa</i>	no effect	Core-tops/plankton tows/sediment traps	MC-ICP-MS	Bootstrap	$\delta^{11}\text{B}_{\text{meas}} = \delta^{11}\text{B}_{\text{lake}} + 0.42 (\pm 2.85) / 0.95 (\pm 0.17)$	5	5	Henahan et al., 2016
<i>O. universa</i>	>425	Core-tops	MC-ICP-MS	Bootstrap	$\delta^{11}\text{B}_{\text{meas}} = \delta^{11}\text{B}_{\text{lake}} + 5.69 (\pm 7.51) / 1.26 (\pm 0.39)$	6	6	Rätzsch et al., 2018
<i>G. bulloides</i>	300-355	Core-top/sediment trap	MC-ICP-MS	Bootstrap	$\delta^{11}\text{B}_{\text{meas}} = \delta^{11}\text{B}_{\text{lake}} + 3.440 (\pm 4.584) / 1.074 (\pm 0.252)$	27	4	Martinez-Boit et al., 2015
<i>G. bulloides</i>	315-355	Core-tops	MC-ICP-MS	Bootstrap	$\delta^{11}\text{B}_{\text{meas}} = \delta^{11}\text{B}_{\text{lake}} + 3.81 (\pm 3.17) / 1.13 (\pm 0.72)$	9	6	Rätzsch et al., 2018
<i>N. pachyderma</i>	150-200	Core-tops	MC-ICP-MS	Bootstrap	$\delta^{11}\text{B}_{\text{meas}} = \delta^{11}\text{B}_{\text{lake}} + 3.38$	9	0	Yu et al., 2013
<i>G. ruber</i>	250-400	Core-tops	MC-ICP-MS	Bootstrap	$\delta^{11}\text{B}_{\text{meas}} = \delta^{11}\text{B}_{\text{lake}} - 9.11 (\pm 0.73) / 0.58 (\pm 0.91)$	5	1	This study; Henahan et al., 2013
<i>G. ruber</i>	250-400	Core-tops	MC-ICP-MS	Bootstrap	$\delta^{11}\text{B}_{\text{meas}} = \delta^{11}\text{B}_{\text{lake}} + 1.23 (\pm 0.59) / 1.12 (\pm 1.67)$	40	2	This study
<i>G. ruber</i>	250-455	Core-tops	MC-ICP-MS	Bootstrap	$\delta^{11}\text{B}_{\text{meas}} = \delta^{11}\text{B}_{\text{lake}} - 11.73 (\pm 0.83) / 0.46 (\pm 0.34)$	11	3	This study; Foster et al., 2008; Henahan et al., 2016; Rätzsch et al., 2018
<i>T. sacculifer (sacc and w/o sacc)</i>	250-400	Core-tops	MC-ICP-MS	Bootstrap	$\delta^{11}\text{B}_{\text{meas}} = \delta^{11}\text{B}_{\text{lake}} + 6.06 (\pm 0.25) / 1.38 (\pm 1.33)$	27	4	This study
<i>T. sacculifer (sacc and w/o sacc)</i>	250-400	Core-tops	MC-ICP-MS	Bootstrap	$\delta^{11}\text{B}_{\text{meas}} = \delta^{11}\text{B}_{\text{lake}} - 4.09 (\pm 0.86) / 0.83 (\pm 0.48)$	5	5	This study; Foster et al., 2008; Rätzsch et al., 2018
<i>N. aderneti</i>	300-400	Core-tops	MC-ICP-MS	Bootstrap	$\delta^{11}\text{B}_{\text{meas}} = \delta^{11}\text{B}_{\text{lake}} - 0.34 (\pm 1.83) / 0.93 (\pm 0.55)$	5	5	This study
<i>N. aderneti</i>	300-400	Core-tops	MC-ICP-MS	Bootstrap	$\delta^{11}\text{B}_{\text{meas}} = \delta^{11}\text{B}_{\text{lake}} - 3.88 (\pm 0.65) / 0.72 (\pm 0.74)$	9	6	This study; Foster et al., 2008
<i>O. universa</i>	400-600	Core-tops	MC-ICP-MS	Bootstrap	$\delta^{11}\text{B}_{\text{meas}} = \delta^{11}\text{B}_{\text{lake}} + 8.01 (\pm 2.23) / 1.38 (\pm 2.67)$	5	7	This study
<i>O. universa</i>	400-600	Core-tops	MC-ICP-MS	Bootstrap	$\delta^{11}\text{B}_{\text{meas}} = \delta^{11}\text{B}_{\text{lake}} + 2.08 (\pm 0.59) / 1.06 (\pm 0.13)$	36	8	This study; Henahan et al., 2016; Rätzsch et al., 2018
<i>G. menardi</i>	400-600	Core-tops	MC-ICP-MS	Bootstrap	$\delta^{11}\text{B}_{\text{meas}} = \delta^{11}\text{B}_{\text{lake}} - 5.36 (\pm 1.36) / 0.65 (\pm 0.76)$	5	9	This study
<i>G. menardi</i>	400-600	Core-tops	MC-ICP-MS	Bootstrap	$\delta^{11}\text{B}_{\text{meas}} = \delta^{11}\text{B}_{\text{lake}} - 6.33 (\pm 2.52) / 0.57 (\pm 1.2)$	3	10	This study
<i>G. tunida</i>	300-400	Core-tops	MC-ICP-MS	Bootstrap	$\delta^{11}\text{B}_{\text{meas}} = \delta^{11}\text{B}_{\text{lake}} - 5.59 (\pm 4.16) / 0.59 (\pm 0.65)$	6	11	This study; Henahan et al., 2016
<i>P. obliquiloculata</i>	300-600	Core-tops	MC-ICP-MS	Bootstrap	$\delta^{11}\text{B}_{\text{meas}} = \delta^{11}\text{B}_{\text{lake}} - 1.99 (\pm 0.13) / 0.82 (\pm 0.27)$	22	12	This study
<i>Deep-dweller</i>	300-600	Core-tops	MC-ICP-MS	Bootstrap	$\delta^{11}\text{B}_{\text{meas}} = \delta^{11}\text{B}_{\text{lake}} - 0.18 (\pm 0.6) / 0.95 (\pm 0.13)$	54	13	This study; Foster et al., 2008; Henahan et al., 2016; Rätzsch et al., 2018